Modeling and Control of Cable-Riding Robots

A Thesis

Presented to the

Graduate Faculty of the

University of Louisiana at Lafayette

In Partial Fulfillment of the

Requirements for the Degree

Master of Science

Ninad Pravin Dhundur

Fall 2013

Modeling and Control of Cable-Riding Robots

Ninad Pravin Dhundur

APPROVED:

Joshua Vaughan, Chair Assistant Professor of Mechanical Engineering	Yucheng Liu Assistant Professor of Mechanical Engineering
Mostafa Elsayed Professor of Mechanical Engineering	Mary Farmer-Kaiser Interim Dean of the Graduate School

ACKNOWLEDGMENTS

This thesis would have remained a dream had it not been for Dr. Vaughan who had given me an opportunity to work on this enthralling project. I owe him for his excellent guidance, understanding, patience, and providing me with an excellent atmosphere for doing research. He encouraged me to not only think individually and independently but also to explore different aspects with different perspectives.

I would like to thank HiBot corp. for providing exclusive information regarding its Expliner inspection robot and contributing greatly for this thesis.

I am also indebted to Graduate School for admitting me into master's program. I would like to thank the department of mechanical engineering for offering me position of graduate assistant, which helped me expand my skills and excel my career. I also thank the department for providing funds for my education.

I would like to express my gratitude to my parents Mr. Pravin Dhundur and Mrs. Priyali Dhundur, and my brother Mr. Rohan Dhundur. They have been always there for me in times of happiness and difficulties, encouraging me to achieve my goals overcoming all the hurdles. I am immensely grateful for their unconditional love that they provided me.

TABLE OF CONTENTS

LIST OF TABLES

LIST OF FIGURES

Chapter I Background and Motivation

1.1 Ropes, Cables and Cable Cars

Ropes or cables are of great importance in various fields like construction, explorations, sports, communication, energy transfer and transportation. Cables provide great tensile strength and elasticity. In the field of electrical engineering, cables are often used for high-voltage overhead and underground power transmission.

Figure 1 shows an example of tensile strength cables can provide. Suspension bridges use cables to hold the deck below. Another common use of cable is the transportation unit called a gondola lift, which is a type of aerial lift supported and propelled by cables from above. An example Gondola is shown in Figure 2. Gondolas consist of a loop of steel cable that is strung between two stations, sometimes over intermediate supporting towers. The cable is driven by a bull-wheel in a terminal, which is connected to an engine or electric motor.

Figure 1. Cable Suspension Bridge [1]

Figure 2. Gondola Lift [2]

Gondolas are often considered continuous systems, since they feature a haul rope which continuously moves and circulates around two terminal stations [3]. The longest ropeway system built in Sweden is 96 kilometers long.

1.2 Cable Vibration

While gondola lifts are an advantageous mode of transportation over difficult terrain, they have certain limitations and many design factors to be considered. As the car moves along the cable, vibration due to the load is inevitable. Vibrations in the cable car systems for passengers are undesirable and can cause discomfort. Cable vibration due to the motion of the moving load thus becomes an important factor to be considered. Cable vibration has been studied for decades. Figure 3 shows various modes of vibration of cables, where L is the span of string and v is the speed of propagation [4]. For applications of cable cars only the first mode of vibration matters the most. There are infinite modes of vibrations, but to determine the amplitude of vibration in cable, only the first mode needs to be studied.

Studies conducted in the past determined the dynamic response of a cable system due to static or harmonic force excitation [5], but little work had been done where the excitation

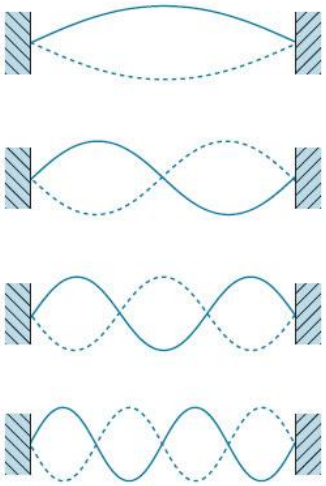

Mode	Wavelength	Frequency
First	$2L$	$v/2L$
Second	L	v/L
Third	$2/3L$	$3v/2L$
Fourth	$L/2$	$2v/L$

Figure 3. Various Modes of String Vibration [4]

is caused due to a moving load on cable. Yi-Ming Wang generated analytical solution for vibration of cable-mass system due to motion of an attached accelerating mass [5]. Marta Knawa and Danuta Bryja worked on non-linear vibrations of ropeway system with moving passenger cabin [6]. They also modeled problems of steeply inclined cableway subjected to moving load and effects of dynamic loads acting on carrying cable in operating ropeway. Brownjohn contributed in dynamics of aerial cableway system, which gives the response of cable to a moving load [7].

Jong-Shyong Wu and Chi-Ching Chen developed a model to determine the dynamic response of a suspended cable due to moving load [8]. Recker developed a model that generates the dynamic response of a taut string to a randomly moving load [9]. Ferreti and Piccardo studied linear vibration induced in an elastic wire by a mass moving with a constant velocity [10]. Metrikine and Bosch proposed a method for calculating steady state response of a two-level catenary to a uniformly moving load [11]. Zoller and Zobory studied the responses caused by fixed and moving loads acting on supported strings and beams [12].

1.3 High-Voltage Overhead Power Transmission Towers and Cables

High-voltage overhead power transmission cables are subject to vibrations as well. Figure 4 shows an image of overhead transmission tower with cables, and Figure 5 shows the structure of high-voltage cable. As transmitting electricity over long distances is necessary, maintaining overhead transmission cables is also a need. Power failures in many grids in the last few decades were due to wear and tear of transmission cables caused by environmental factors.

Maintenance of such high voltage transmission cables is a dangerous and important task. Most transmission cables are inspected by humans who crawl along the cables, as shown in Figure 6. A low flying helicopter carries them over the cables and lowers them onto the cables. This increases the inspection time and is very dangerous. In Japan, during inspection, transmission lines are interrupted by cutting off electricity through those cables until inspection has been carried out. The total cost of interrupting power lines estimate to be as high as 119 billion US dollars annually [13].

Figure 4. High-Voltage Power Transmission Tower and Cable [14]

Figure 5. High-Voltage Power Transmission Cable [15]

Figure 6. Crawling along High-Voltage Power Transmission Cables for Inspection (A still image from video) [16]

1.4 Power Line Inspection Robots

To make the high-voltage power lines inspection less dangerous for humans, engineers have developed inspection robots. These robots can inspect power lines without interrupting the power. Xiaohui Xiao, Gongping Wu, Hua Xiao and Jinchun Dai developed a power line

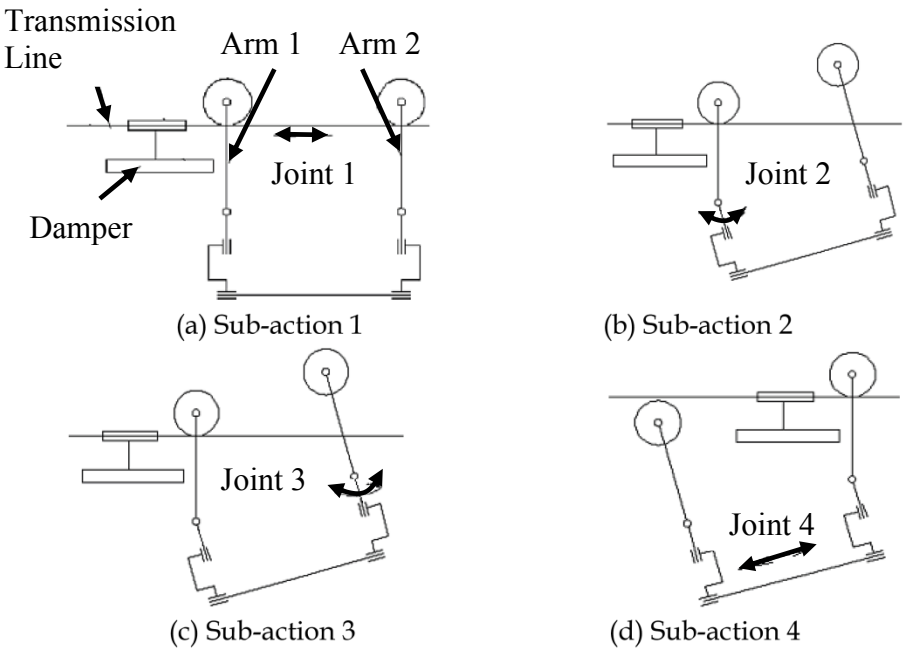

Figure 7. ARCR Action Programming for Damper-Overcoming [17]

inspection robot named Auto Rolling/Crawling Robot (ARCR) [17]. ARCR inspects high-voltage live power lines and can traverse obstacles that crop up on the cable.

The process of traversing the damper on the cable by ARCR is shown in four sub-actions in Figure 7. In sub-action 1, the two wheels travel along the cable and the arms are parallel to each other. In sub-section 2, joint 2 rotate, lifting one of the wheel and arm. In sub-action 3, joint 3 rotate by 180 degrees. In sub-action 4, arm 2 translates along joint 4. Then arm 2 lifts up and sits the wheel on cable. This same procedure is followed for the other wheel. This way, ARCR traverses the damper on transmission lines. Though ARCR is capable of inspecting power lines, it can only inspect one power line cable at a time. A prototype has been developed by Wuhan University at China [17].

Another such inspection robot, named LineScout shown in Figure 8, was developed by Serge Montambault and Nicolas Pouliot [18]. LineScout travels along a single power

cable at a time and is made up of three frames [18]. The first frame is the wheel frame which consists of two wheels, shown in dark color in Figure 9. The arm frame is equipped with two arms and two grippers, shown in light color. The center frame (white circle) links the first two links which allows them to slide over each other and pivot. As the robot reaches an obstacle, the arm frame clamps itself on the cable allowing the wheel frame to slide over center frame and transfer to other side of the obstacle. To complete this action, the wheel frame flips down by 180 degrees. As the wheel frame is transferred to other side of the obstacle, it flips back by 180 degrees and the wheels rest on cable again. This way LineScout traverses any obstacles on the cable.

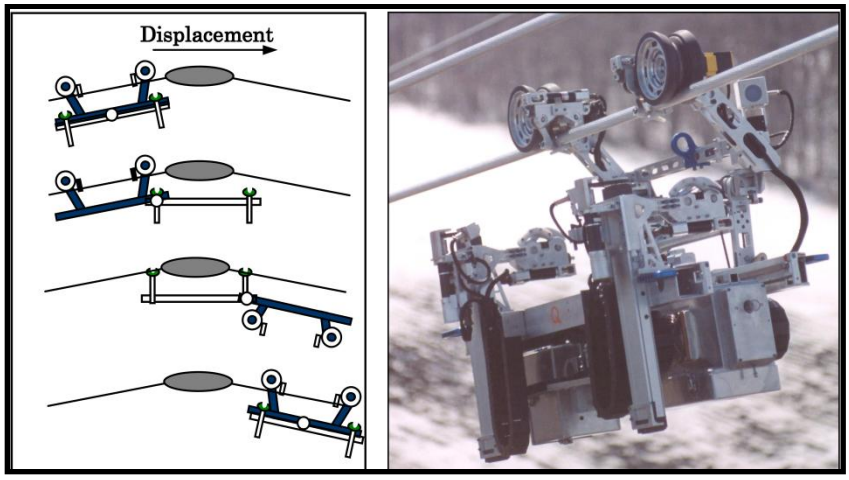

a) Obstacle-Clearing Sequence b) The LineScout Mobile Platform

Figure 8. The LineScout [18]

1.4.1 HiBot's Expliner Robot

HiBot (www.hibot.co.jp/), a Tokyo-based company, along with Japan's Kansai Electric Power Co., developed a field robot that can inspect several power cables at once. HiBot's Expliner robot [20], shown in Figure 9, can examine live high-voltage power transmission cables. Expliner is designed to roll along the upper cables in a bundle of four held in place by

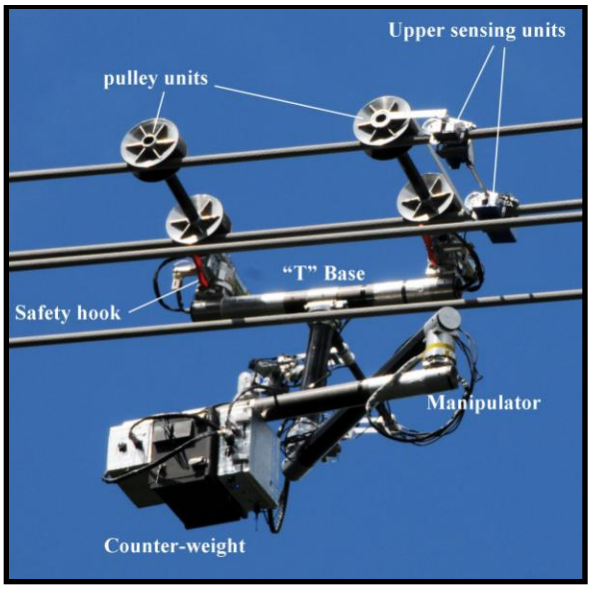

Figure 9. HiBot's Expliner Robot [19]

Figure 10. Expliner Overcomes Cable Spacers of Different Shapes and Sizes [19]

spacers, which are square shaped half meter wide, shown in Figure 10. These spacers are located every 30m along the transmission line. Expliner can travel along live cables carrying up to 500 kilovolts of potential difference.

Expliner is similar to four-wheeled cable car that rolls along the cables. A manipulator arm on one side of robot carries a counter-weight for balance and shifting the center of gravity. Expliner has four pulleys that ride along the cable. Each pair of pulleys is

connected by an axle. A pair of pulleys and axle collectively makes one pulley unit. Figure 9 shows detailed image of Expliner, which shows the pulley units, manipulator arm, and counter-weight. An on-board camera inspects the cables, spacers, and clamps. Figure 11 shows the structural condition of cable spacers, captured by the on-board camera. The on-board camera inspects the cable as shown in Figure 12. It gives detail surface condition of cables and any defects found are recorded for maintenance.

Expliner encounters certain obstacles on cable during its travel along the high-voltage cables. One such obstacle is the spacer, as shown in Figure 10. Expliner can relatively easily traverse over these spacers. The important concern is the suspension clamps that hold the cables and block the way of Expliner, as shown in Figure 13. Expliner has to overcome this obstacle for uninterrupted inspection.

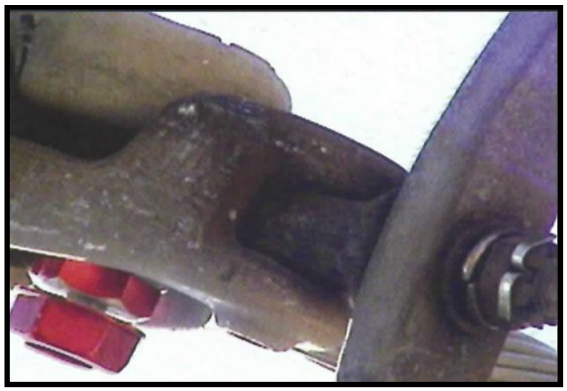

Figure 11. The Structural Condition of Spacers Confirmed in Detail with On-Board Camera [19]

Figure 12. Sensors Placed around the Cables for Detailed Inspection of Surface Conditions [19]

Figure 13. Suspender Clamps Holding the Power Transmission Cables [20]

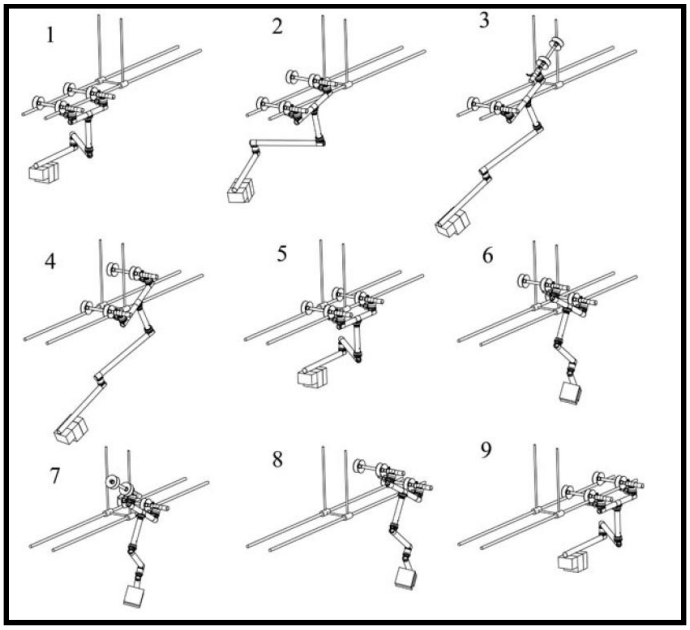

Figure 14. Sequence of Motion of Expliner Robot Overcoming Clamp Suspender [20]

Figure 14 shows the acrobatic mode that Expliner uses to traverse these obstacles. To traverse suspender clamps, Expliner uses the counterweight on the manipulator arm to shift the center of gravity of robot, this helps to lift either the front axle or back axle. The axle then

Figure 15. An Ingenious Balance Control Concept to Negotiate Suspender Clamps [19]

rotates around, like pushing away a door, and thus moving out of the way of suspension clamp. Expliner then continues its travel along the cable on a single pulley unit until the axle completely passes the clamp, and then the axle is pulled down back to the cable. This procedure continues the same for the other axle to clear its way. Figure 15 shows Expliner during its acrobatic mode.

Though the design of the Expliner is impressive, it has some limitations. These limitations have been brought into light in next section, and solutions have been presented to make the inspection operation of Expliner even more robust.

1.5 Conclusion

In this chapter, importance of cables in various fields was explained. It was shown how cables are important for transportation via cable cars. But these cable cars are subjected to vibration during its travel. Vibration in cable cars can be dangerous.

The high voltage power transmission was also discussed in this chapter. Since these power lines need to be inspected regularly, researchers developed inspection robots. Since

these inspection robots travel along the cable, some vibrations are induced in the cable. This makes the inspection task difficult.

A mass accelerating on a cable fixed at both ends, induce vibration in the cable [5], [8]. This can affect the inspection operation of the Expliner. This vibration in the cable is studied in Chapter 2. A new simple cable mass model is proposed, this model gives the dynamic response of the cable vibrations due to traveling load. Also it is important for the Expliner to be as stable as possible, since it travels on just single pulley unit, it is subjected to rocking oscillations. Rocking oscillations makes it difficult for sensors and camera to gather detailed information of surface conditions of cables and spacers. This rocking oscillation induced in Expliner is studied in Chapter 3, and a method is suggested to control and reduce it.

Chapter II Cable Modeling

2.1 Developing a Cable Model

HiBot's Expliner travels along the cable inducing vibrations in the cable and possibly in Expliner. To study these cable vibrations, existing cable models were studied which give the transient dynamics of cable-mass system due to motion of attached accelerating mass [5], [8], [9], [10], [11], and [12]. Also, a mathematical model that gives the non-linear vibrations of ropeway systems with moving passenger cabins was studied [6]. These models used complex partial differential equations to obtain the dynamic response of the cable. Using these models, it is difficult to create a control. For many applications of cable systems, the first mode of vibration is dominant. Other higher modes of vibrations do not contribute significantly to the vibration. Hence, a simpler cable model was developed to use for control design. This simple model only used the simple cable-mass system to generate the dynamic response. This model captures the dominant dynamics of the system, which are required to design a control system.

Figure 16 shows a cable fixed at two ends. It is freely hanging under its own weight, forming a catenary curve. To mimic the action of this cable a new simple cable model, shown in Figure 17, is proposed to represent the dominant dynamics of the cable. The cable is modeled as series of bodies, each connected by two springs from the fixed supports. The bodies are arranged in catenary shape by adjusting the spring stiffness for each body. In this thesis, this model is called the two spring-mass model.

For all simulations, the number of bodies used was 1000 per meter. Figure 17 shows only a few number of bodies, but to simulate this model, 1000 bodies per meter were used.

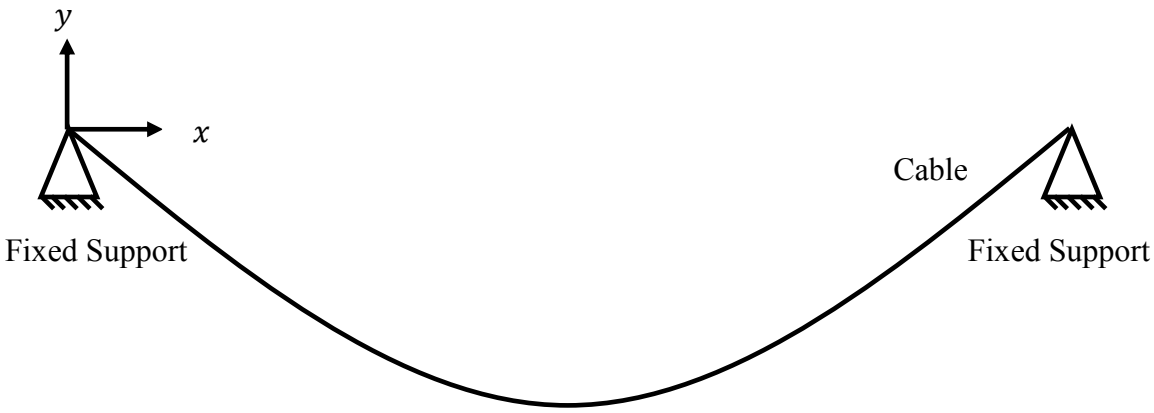

Figure 16. Graphical Model of Cable Fixed at Both Ends

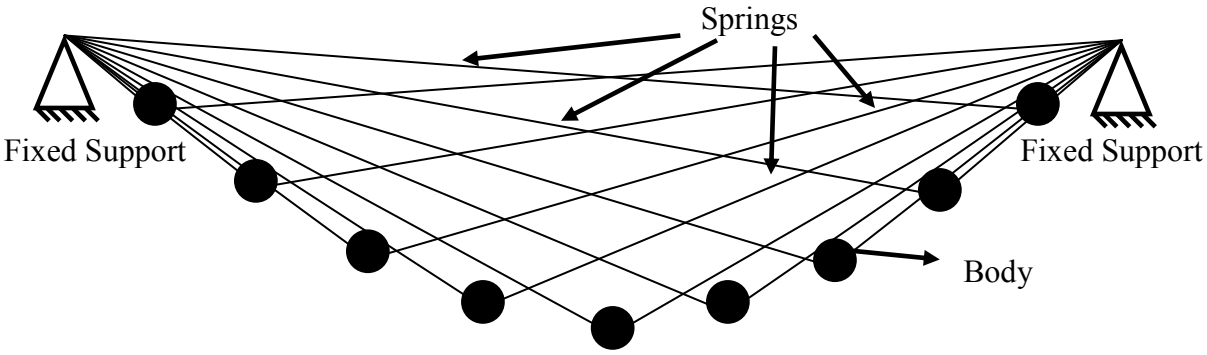

Figure 17. Each Body Attached by Two Springs from Fixed Ends

Assumptions made in developing two spring-mass model include:

1. Springs obey Hooke's law of elasticity.
2. The bodies are not physically attached to each other.
3. The motion of bodies is restricted to vertical motion.

The stiffness of spring is arranged such that the bodies form catenary curve of cable in its equilibrium position.

2.1.1 Developing Two Spring-Mass Model

Figure 18 shows the curve formed by cable fixed at both ends. Since the cable is hanging by its own weight it forms a catenary curve. Figure 18 shows the co-ordinates of the fixed ends and the center of cable. A model was created to mimic this cable. In Figure 18, L is the length of span and s is the sag. The general equation of catenary curve shown in Figure 18 is:

$$y = a\cosh\left(\frac{x}{a} - b\right) + c \quad 0 < x < L \tag{1}$$

where $a,\ b$ and c are parametric constants, y is the vertical displacement, and x is the horizontal distance. To find $a,\ b$ and c, co-ordinates shown in Figure 18 were substituted into (1):

$$0 = a\cosh(-b) + c \tag{2}$$

$$0 = a\cosh\left(\frac{L}{a} - b\right) + c \tag{3}$$

$$-s = a\cosh\left(\frac{L}{2a} - b\right) + c \tag{4}$$

Equations (2), (3), and (4) are solved using MATLAB solver function for given values of L and s. Values of a, b and c obtained from MATLAB solver function was used to develop the equation of catenary (1).

The length of the cable curve from an arbitrary point x_i to x_f for span length L and sag s in Figure 18 is given in (5). This equation gives the curved length of cable between any two points on the cable.

$$curve\ length = a\left[\sinh\left(\frac{x_f}{a} - b\right) - \sinh\left(\frac{x_i}{a} - b\right)\right] \tag{5}$$

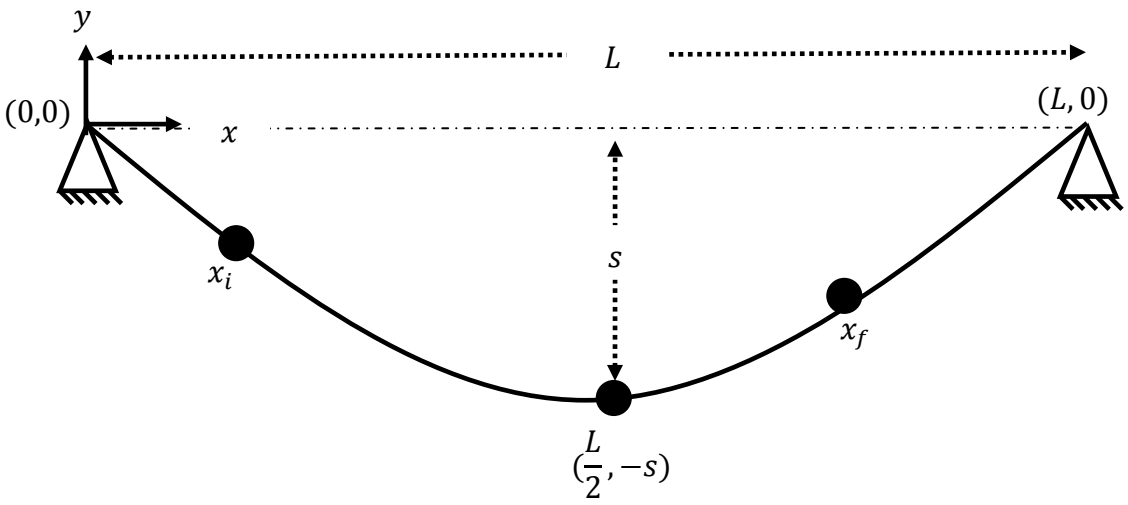

Figure 18. Cable Forming Catenary Curve

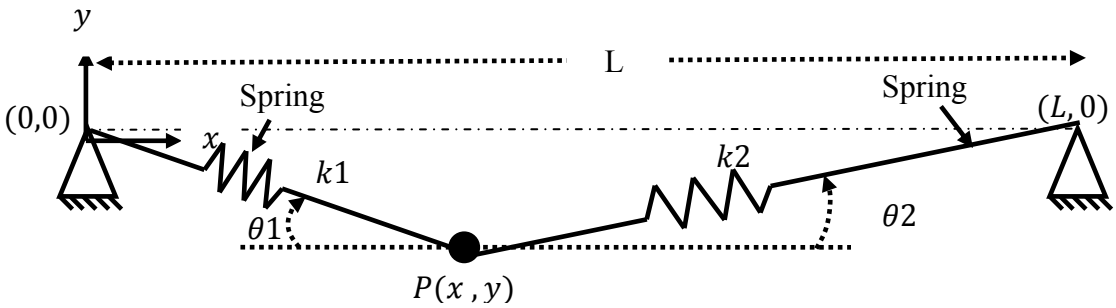

Figure 19. Two Spring-Mass Model

Figure 19 shows a point or a body, attached by two springs. This body $P(x, y)$ is an arbitrary point that lies on the cable or catenary curve.

The curved length of cable from fixed end $(0, 0)$ to point $P(x, y)$ is:

$$l1 = a\left[\sinh\left(\frac{x}{a} - b\right) - \sinh\left(\frac{0}{a} - b\right)\right] \tag{6}$$

The curved length of cable from point $P(x, y)$ to fixed end $(L, 0)$ is

$$l2 = a\left[\sinh\left(\frac{L}{a} - b\right) - \sinh\left(\frac{x}{a} - b\right)\right] \tag{7}$$

spring constant value $k1$ for spring is:

$$k1 = \frac{AE}{l1}(\sin\theta 1)^2 \tag{8}$$

where A is the cross-sectional area of cable and E is modulus of elasticity of the material of cable and

$$\theta 1 = \tan^{-1}\left(\frac{y}{x}\right) \tag{9}$$

where y is the equation of catenary curve as given in (1). Spring constant value $k2$ for spring is:

$$k2 = \frac{AE}{l2}(\sin\theta 2)^2 \tag{10}$$

where,

$$\theta 2 = \tan^{-1}\left(\frac{y}{L-x}\right) \tag{11}$$

The general equation of motion for a spring-mass system along y direction is:

$$m\ddot{x} + c\dot{x} + kx - mg = 0 \tag{12}$$

where m is the mass of load, c is the damping constant, and k is the spring constant. For case shown in Figure 20, the equation of motion of the equivalent spring-mass system is written as:

$$m\ddot{x} + C_{eq}\dot{x} + K_{eq}x - mg = 0 \tag{13}$$

where m is the mass of load, C_{eq} is equivalent damping constant, and K_{eq} is the equivalent spring constant of two springs $l1$ and $l2$, as shown in Figure 20. An equivalent of two spring -mass model is shown in Figure 20, where the K_{eq} is the equivalent of the two springs. Figure 21 shows the equivalent of all two spring-mass systems.

The K_{eq} is the sum of Equations (8) and (10)

$$K_{eq} = \frac{AE}{l1}(\sin\theta 1)^2 + \frac{AE}{l2}(\sin\theta 2)^2 \tag{14}$$

The entire equation of K_{eq} was developed by substituting the parameters $l1, l2, \theta 1$, and $\theta 2$ into (14). Equation for equivalent spring stiffness,K_{eq}, in Figure 21, is written as:

$$K_{eq} = \frac{AE}{\left(a\left[\sinh\left(\frac{x}{a}-b\right)-\sinh(-b)\right]\right)}\sin\left(\tan^{-1}\left(\frac{a\cosh\left(\frac{x}{a}-b\right)+c}{x}\right)\right)^2 + \frac{AE}{\left(a\left[\sinh\left(\frac{L}{a}-b\right)-\sinh\left(\frac{x}{a}-b\right)\right]\right)}\sin\left(\tan^{-1}\left(\frac{a\cosh\left(\frac{x}{a}-b\right)+c}{L-x}\right)\right)^2 \tag{15}$$

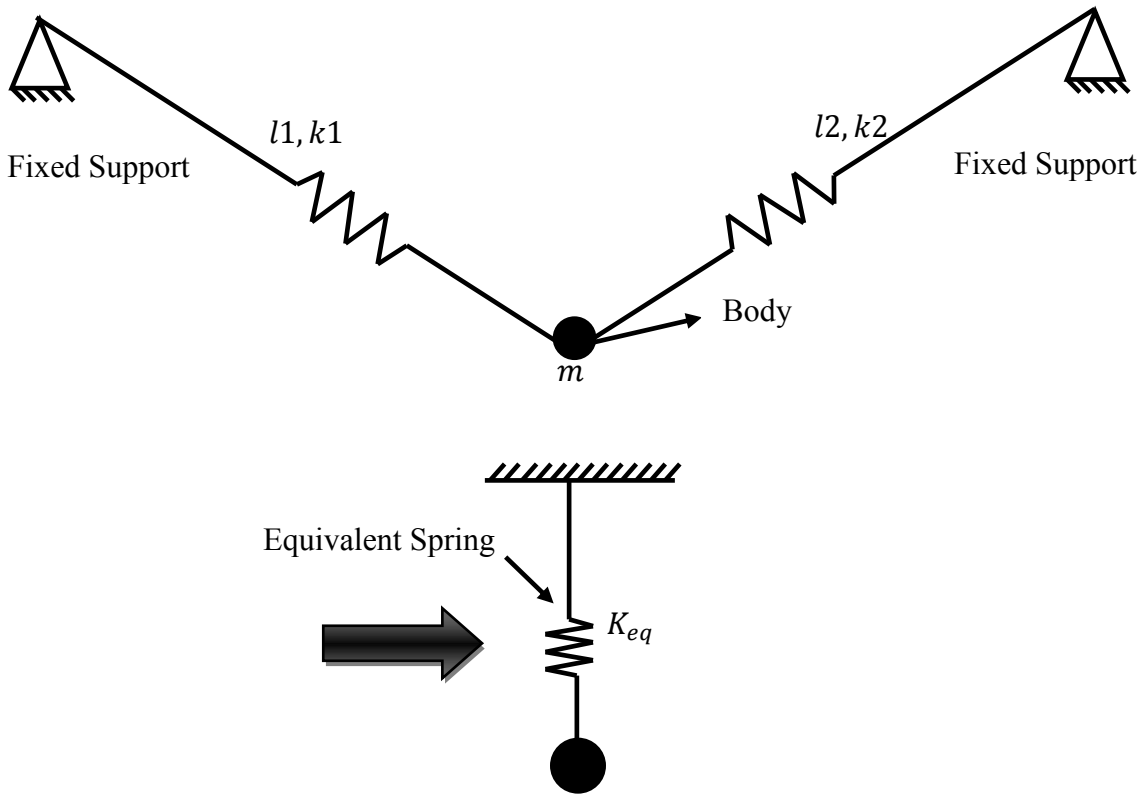

Figure 20. Equivalent System of Two Spring-Mass System

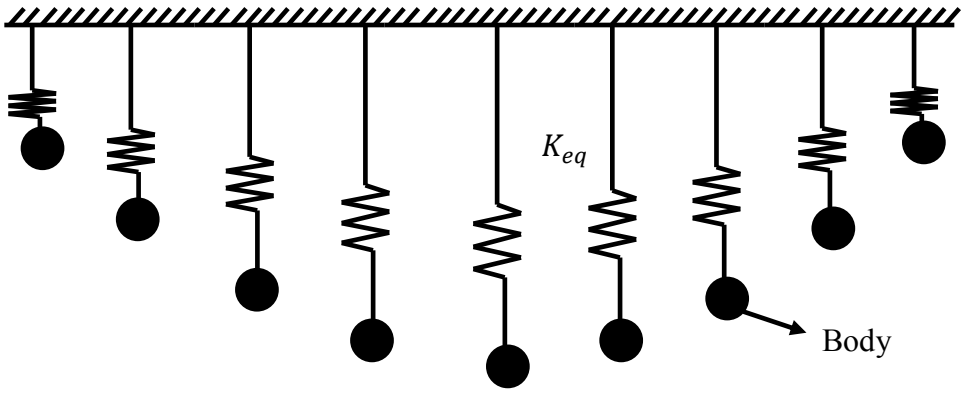

Figure 21. Equivalent Spring-Mass System of all Bodies

The stiffness of springs is maintained in such a way that the bodies form exact shape of catenary curve in its equilibrium position. This way the bodies can mimic the action of a cable.

2.2 Frequency Analysis

The natural frequency of the two spring-mass system is:

$$\omega(x) = \sqrt{\frac{K_{eq}}{m}} \tag{16}$$

It is a function of x, other parameters L, m, s, a, b and c are constants for a given system. Various frequency plots were generated in MATLAB to give a better idea of the frequency of the system. Simulations are run for the values given in Table 1. A new dimensionless, normalized parameter X is introduced, defined as a ratio of the x co-ordinate of location of mass on cable to the span of the cable. That is, $X = {}^{x}/_{L}$, which varies from 0 to 1. X defines the location of load on cable. The natural frequency of the system was determined with use of (15), (16), and parameters given in Table 1. The results from simulation for natural frequency of the system are shown in Figure 22.

To investigate the nature of natural frequency for various high voltage power transmission cables, a study was made for 7 configurations of cable length, span and sag, which are commonly found and reported by an IEEE task force [21]. Configurations of cable curve used for simulations are shown in Table 2. Using configurations given in Table 2, simulations were run for X between 0.2 and 0.8, as shown in Figure 23.

Table 1: Cable and Load Parameters

Parameters	Values
Cable span (L)	$450ft \approx 137m$
Cable sag (s)	$8.1ft \approx 2.5m$
Mass of load (M)	$90kg$
Radius of cable	$0.025m$
Elasticity modulus (E)	$180e9\, N/m^2$

Table 2: Cable Parameters

	Set 1	Set 2	Set 3	Set 4	Set 5	Set 6	Set 7
Cable span (ft)	450	650	750	850	950	1150	1500
Cable span (m)	137.1	198.1	228.6	259	289.6	350.5	457.2
Cable sag (ft)	8.1	16.2	22.2	26.9	33.4	50.2	78.2
Cable sag (m)	2.5	5	6.8	8.2	10.2	15.3	23.8

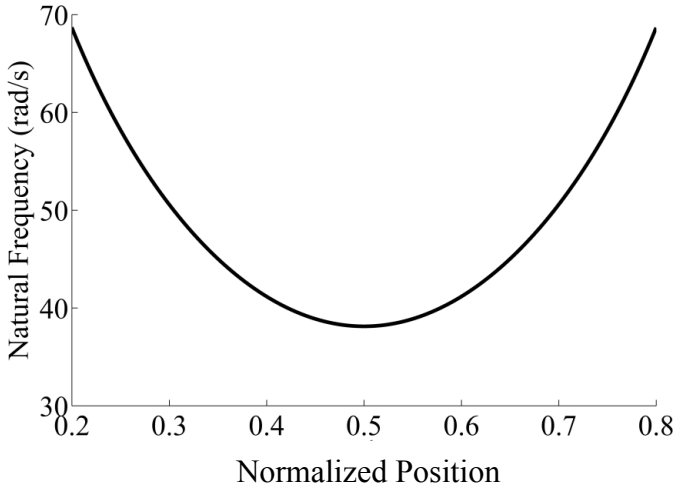

Figure 22. Natural Frequency of the System, for X between 0.2 and 0.8

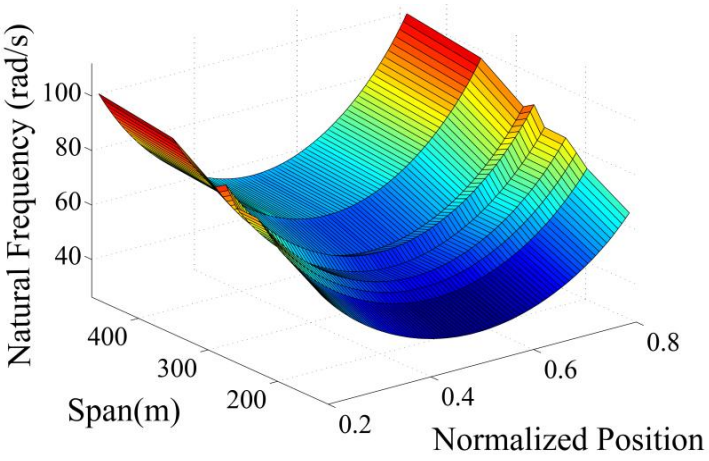

Figure 23. Natural Frequency of the Two Spring-Mass Model

2.3 Dynamic Response of Cable Due to Moving Load

In the previous subsection, a mathematical model of cable was created. The model was used to determine the frequency and amplitude of vibrations caused by load traveling on cable at constant velocity. A method was proposed to simply model a load traveling on cable. The algorithm steps in MATLAB to determine the dynamic response of load traveling on cable using ode45 is:

1. Initially, the load is at any arbitrary point $Q(X)$ on cable at equilibrium, where $X = {}^{x}/_{L}$, which varies from 0 to 1.
2. The load travels to a given direction along cable from this point, at given velocity.
3. Let the load travel with increment of distance d in time dt, where d is 0.001.
4. The equilibrium position of load at $Q(X)$ becomes the end condition of load at this point. The condition of load includes information of its position and velocity.
5. As the load moves forward from $Q(X)$ to $Q(X) + d$ in time dt, which depends on velocity of moving load, the end condition of load at $Q(X)$ becomes the input for the initial condition when load moves to $Q(X) + d$.

6. Then, as load moves to point $Q(X) + 2d$, the end condition of load at $Q(X) + d$ becomes the initial condition for load at point $Q(X) + 2d$.
7. This continues until the desired total distance is traveled.

The algorithm for dynamic response of cable is shown in Figure 24. In Figure 24, $Q(X)$ is arbitrary starting point of moving load on cable where it begins its travel, E.C. is the end condition of the body, I.C. is the initial condition of the body and n is a natural number.

In Figure 24, let the end conditions of point $Q(X)$ be $(a1, v1)$, where a is the displacement and v is the velocity. Initial condition as input for point $Q(X) + d$ becomes $(a1, v1)$ after time dt. Let the end conditions of point $Q(X + d)$ be $(a2, v2)$ which in turn becomes initial condition as input for point $Q(X) + 2d$ after time $2dt$. Every point $Q(X) + nd$, has a different value of spring constant depending on its location on the catenary curve, since the spring constant K_{eq} is a function of x. Since the spring constant K is different at each point, the end conditions of each point will be different than that of preceding point. Thus by obtaining all values of displacement at each point, that is $a1$, $a2$, $a3$ up to an at location $Q(X), Q(X + d), Q(X + 2d)$ up to $Q(X + nd)$, the path traced by moving load on cable is obtained. An imaginary line was defined by all displacements at each point as shown in Figure 25, path traced by moving load on cable is this imaginary line. Thus, the dynamic response of cable vibration caused by a moving load P was determined.

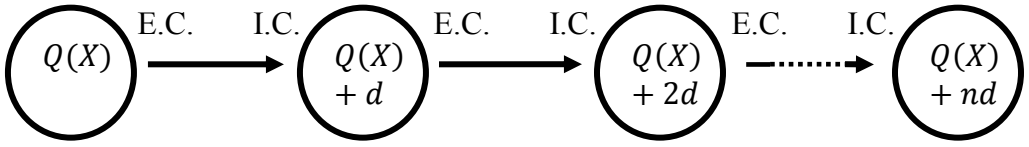

Figure 24. Algorithm for Dynamic Response

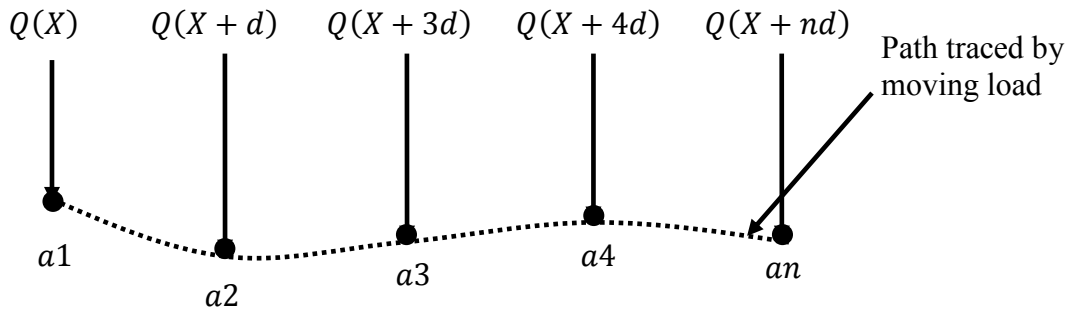

Figure 25. Displacement of Cable Due to Traveling Load

2.3.1 Verifying the Two Spring-Mass Model

To verify the proposed simplified cable model, it was compared to a widely-accepted model of loads moving along flexible cables. Graff and Apaydin extensively researched on moving loads on supported beams. Their research on moving loads on elastically-supported beams gives the response and its time rate of change of a simply supported beam to a moving concentrated load. A load traveling on elastic cable is shown in Figure 26. A simply-supported beam model is used to compare the results with cable model. For comparison, the power line cable has as a plane circular cross section like a rod. In the beam model, the cross sectional area and the moment of inertia for circular rod is used to model the high-voltage power line cable. For comparison, the cable strands are neglected and treated as a uniform rod. The high-voltage power lines have very high stiffness which makes it possible to compare the new cable model with beam model. The solution of simply-supported cable traversed by a load is analogous to that of simply supported beam, as given in (17) [22].

Figure 26 shows a load P traveling along beam with constant velocity v. x is the distance traveled by load along the beam and t is the time. The response of Apaydin's model of load traveling along beam shown in Figure 26 is [23, 24]:

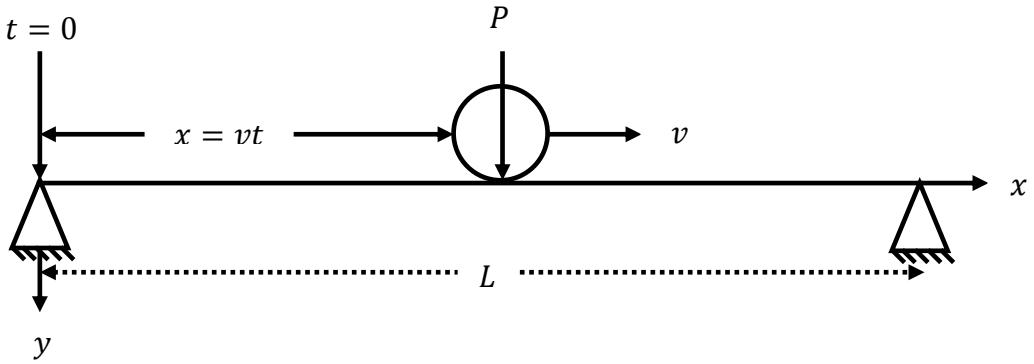

Figure 26. Simply Supported Beam Carrying Moving Concentrated Load

$$y(x,t) = \frac{P}{2\pi^2 m_b l}\left[\sum_{j=1}^{\infty} sin\ 2\pi jft\ - (jf/f_j)\sin 2\pi f_j t\right] sin\frac{j\pi x}{l} \tag{17}$$

$$f_j = \frac{1}{2\pi l^2}\left[\frac{EI\pi^4 j^4}{mb}\right]^{1/2} \tag{18}$$

$$f = \frac{j\pi v}{2\pi l} \tag{19}$$

The parameters given in (17), (18), and (19) are explained in Table 3.

Table 3: Parameters of Beam Model

Parameter	Parameter Details
y	System response
L	Length of beam
P	Weight of moving load
m_b	Mass per unit length of beam
f	Fundamental frequency
f_j	j^{th} Fundamental frequency
v	Velocity of moving load
E	Modulus of elasticity of beam
I	Area moment of inertia of beam

Table 4: Cable and Moving Load Parameters

Parameters	Values
Young's Modulus (E)	180e9N/m^2 (for steel)
Density	76980N/m^3 (for steel)
Radius	0.05m
Load (P)	90kg
Span (L)	131m

To compare the results produced by the two spring-mass model and the beam model, the values in Table 4 were used for simulation. The load used for simulation was 90kg, since that is the approximate weight of Expliner. Simulations were run for varying velocity. Figure 27, 28, and 29 compare the dynamic response of the two spring-mass model to the beam model with velocities $0.3m/s$, $0.38m/s$, and $0.43m/s$, respectively. To find the deviation of result from the beam model, the root-mean-square-error (RMSE) was calculated for each result. The RMSE value is shown in Table 5. RMSE is less than $0.01m$, which is negligible considering entire length of span which is $131m$.

Table 5: Root-Mean-Square-Error over Entire Span

Velocity	Root-mean-square-error
$0.3m/s$	$0.0037m$
$0.38m/s$	$0.005m$
$0.43m/s$	$0.005m$

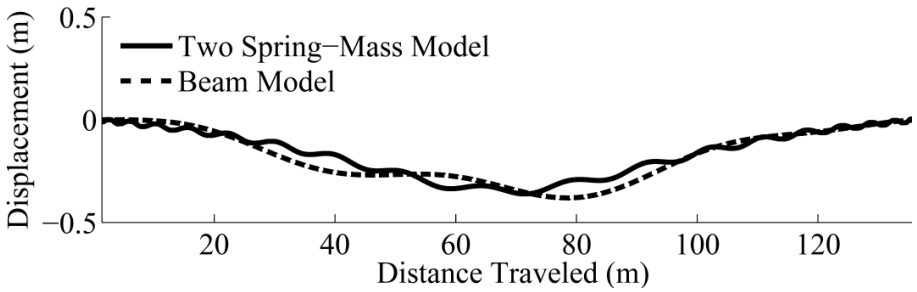

Figure 27. Dynamic Response of Cable Due to Moving Load for Velocity $0.3m/s$

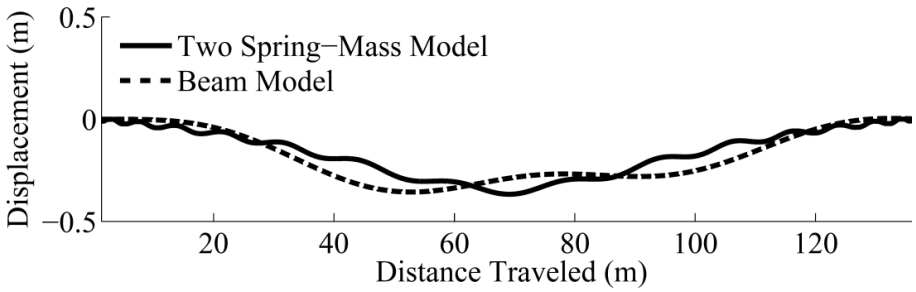

Figure 28. Dynamic Response of Cable Due to Moving Load for Velocity $0.38m/s$

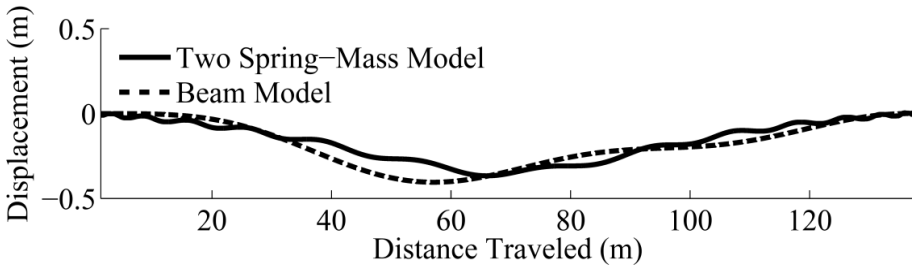

Figure 29. Dynamic Response of Cable Due to Moving Load for Velocity $0.43m/s$

Simulations were run for velocities between $0.3m/s$ and $0.43m/s$ and length of spans between $131m$ and $472m$. The root-mean-square-error calculated from the simulations are shown in Figure 30. It is noted that root-mean-square-error-increases with increase in velocity and length of span. The percentage root-mean-square-error between lengths $131m$ and $472m$ was calculated using (20). The percentage root-mean-square-error ranges between 0.0027% and 0.46% for length of span between $131m$ and $472m$. A maximum percentage root-mean-square-error recorded is 0.46%. Since, this percentage root-mean-square-error is less than 0.5% and the two spring-mass model was used for further investigations.

$$\%RMSE = \frac{RMSE}{Span}100\% \tag{20}$$

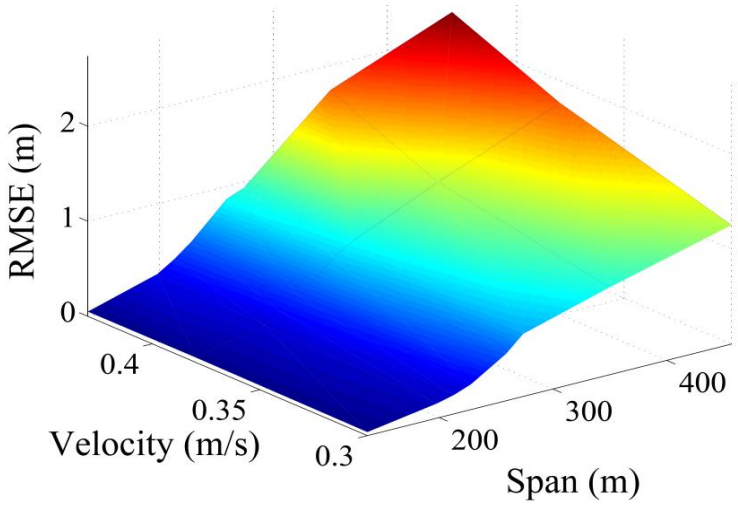

Figure 30. Root-Mean-Square-Error (RMSE) for Varying Velocity and Span

Results from simulations show that the new, two spring-mass model closely matches with the beam model, with a maximum %RMSE of 0.46%. Thus, a successful, new, and simple cable model is created.

2.4 Effect of Cable Vibration on Expliner's Inspection Operation

As explained in previous chapter, Expliner travels along high voltage power transmission cables for inspection with sensors. Expliner enters into an acrobatic mode to traverse suspended clamps. During its acrobatic mode, Expliner travels on single pulley unit to traverse the suspended clamps. Acrobatic mode begins about $2m$ to $3.5m$ before the suspender clamp on the cable. Since, during the acrobatic mode, Expliner travels only on single pulley unit, it is prone to rocking oscillations. These rocking oscillations are unwanted for safe inspection operation. Vibrations in the cable due to Expliner's travel along it may induce further rocking oscillations.

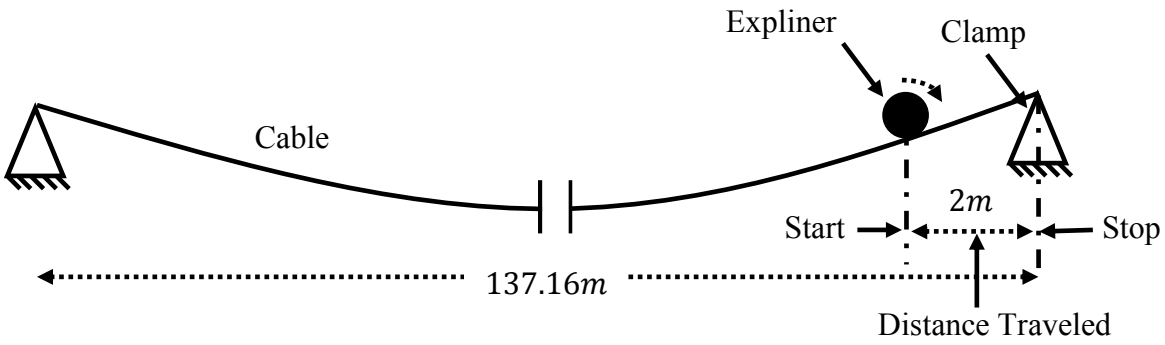

Figure 31. Expliner Traveling Along Cable on Single Pulley Unit

To investigate if vibrations in the cable affects Expliner's operation, a study was made where a load travels $2m$ to 3.5m from the end of cable towards the suspended clamp. Figure 31 shows how Expliner travels along the cable on single pulley unit during acrobatic mode. Expliner begins its acrobatic mode $2m$ from the clamp, but it may be required to begin the acrobatic mode more than $2m$ before the clamp. Hence, dynamic response of cable was simulated for distance traveled between $2m$ and $3.5m$ from the clamp.

The results of dynamic response of cable generated by two spring-mass model and the beam model are shown in Figure 32. In Figure 32, Expliner begins its acrobatic mode $2m$ from the clamp on cable span of length $137.16m$ $(450ft)$ with velocity $0.38m/s$.

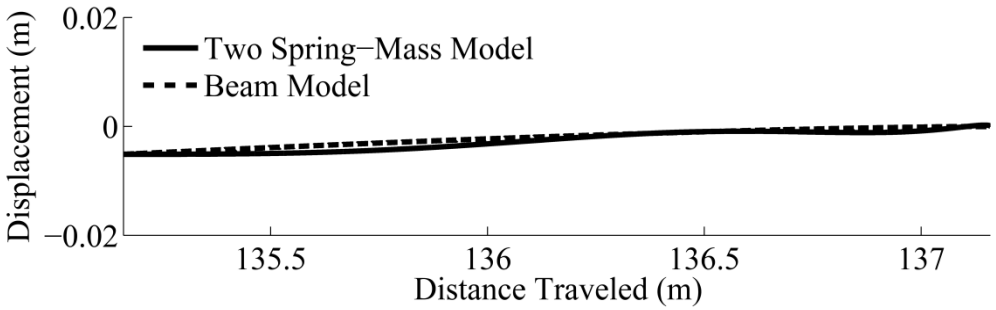

Figure 32. Vibrations in Cable for Distance Traveled $2m$ and Velocity $0.38m/s$

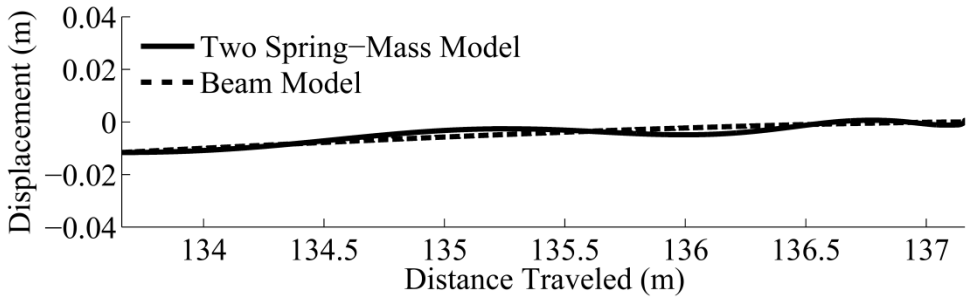

Figure 33. Vibrations in Cable for Distance Traveled $3.5m$ and Velocity $0.38m/s$

The results in Figure 32 show very little vibration in the cable. Error is noted from results obtained with two spring-mass model. The root-mean-square-error for this condition is noted to be $0.00076m$. The percentage root-mean-square-error is 0.0005%, which is negligible.

Simulations were run by varying the distance traveled during acrobatic mode and its velocity. Figures 32, 33 34, and 35 shows the dynamic response of cable for distance traveled between $2m$ and $3.5m$ and velocity between $0.38m/s$ and $0.43m/s$. In these figures, the vibration amplitude is less than 0.1mm. Since Expliner can travel at a velocity as high as $0.43m/s$, a maximum vibration amplitude of 0.1mm can be expected near the end of cable. This little vibration in cable near the suspended clamp does not affect the rocking oscillation in Expliner during its acrobatic mode.

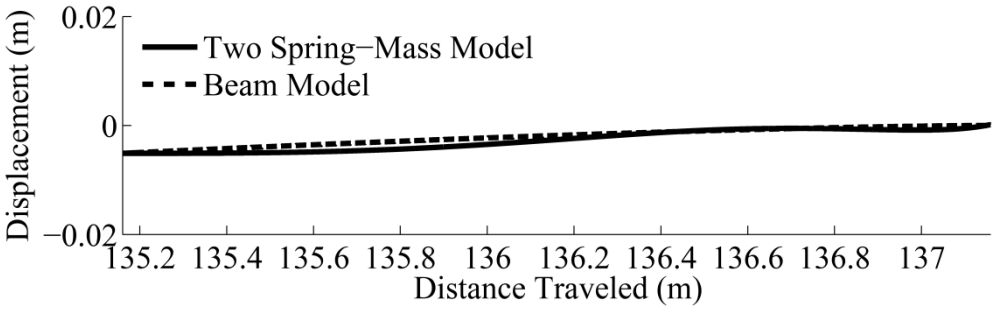

Figure 34.Vibrations in Cable for Distance Traveled $2m$ and Velocity $0.43m/s$

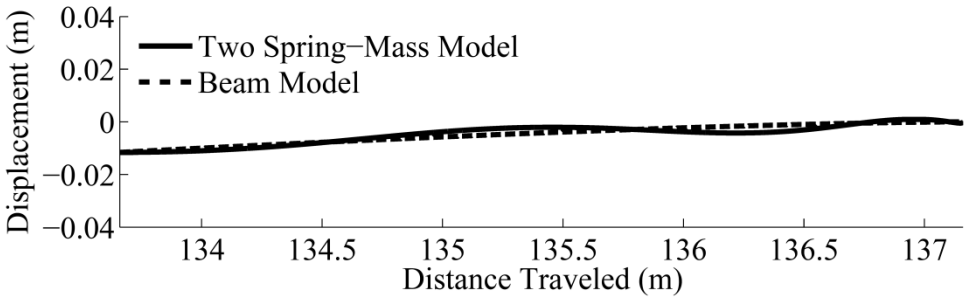

Figure 35. Vibrations in Cable for Distance Traveled $3.5m$ and Velocity $0.43m/s$

To investigate the vibrations induced in cable during Expliner's travel in its acrobatic mode for varying length of span, simulations were run by varying this parameter as well. The maximum vibration amplitude was about 1mm. Also, for this simulation, the root-mean-square-error is noted between the beam model and two spring-mass model. Surf plots for the same are shown in Figure 36 and 37 for velocity $0.38m/s$ and $0.43m/s$, respectively. The root-mean-square-error observed was less than $0.015m$ for all cases and the calculated percentage root-mean-square-error was less than 0.003%.

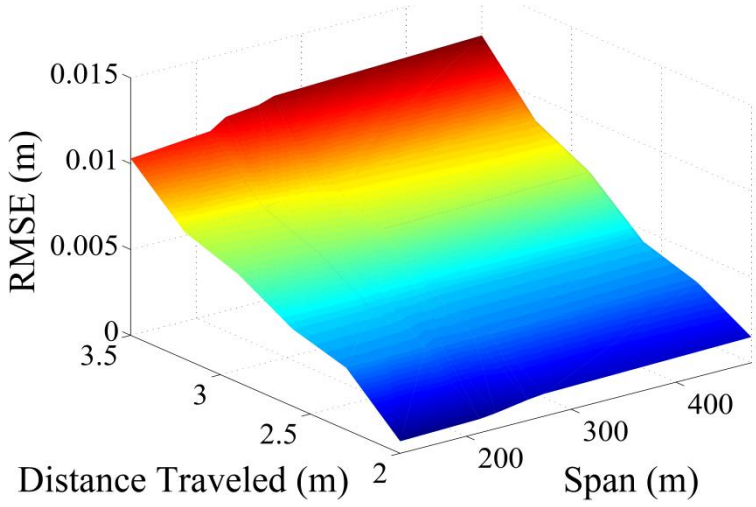

Figure 36. Root-Mean-Square-Error for Velocity $0.38m/s$

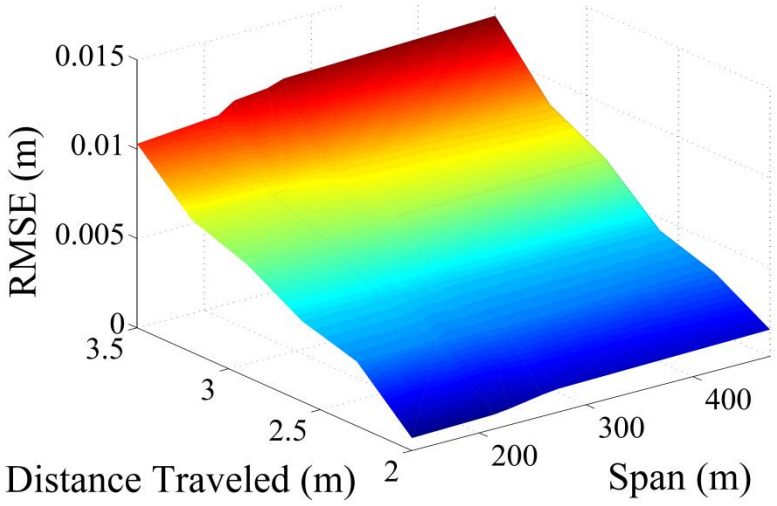

Figure 37. Root-Mean-Square-Error for Velocity $0.43m/s$

Though little amount of vibration in cable, which is less than 1mm, does not affect the rocking oscillations of Expliner, it is necessary to investigate the rocking oscillations induced in Expliner due to its travel on the cable on single pulley unit during its acrobatic mode. The rocking oscillations are induced in Expliner due to its design. A detailed motion of Expliner in its acrobatic mode is studied in Chapter 3, and the rocking oscillations induced were simulated and a method is suggested to control these rocking oscillations.

2.5 Conclusion

To derive the dynamic response of cable vibrations due to traveling mass, various cable models were studied. However for control design, a simpler model was desired. A new, simple mathematical model of suspended cable was proposed, called the two spring-mass model. This two spring-mass model captures the dominant dynamics of the system which can help design a simple control system. Using this model, the natural frequency of the cable was determined. The simulation results from this model were compared with results from a beam model. For high-voltage power lines, a maximum % RMSE was noted to be 0.46%. It was

concluded from this study that, the two spring-mass model can be used for investigations of dynamic response of cable caused by moving load with very little error.

Chapter III Controlling Oscillation in Cable Riding Robots

Cable riding gondolas or robots can undergo significant amount of rocking oscillations during their travel along the cable, which is unsafe. One promising technique to reduce this unwanted oscillation is input shaping.

3.1 Input Shaping

Input shaping is a method of command filtering that allows many oscillatory systems to be moved without residual vibration. Input shaping is implemented by convolving a series of impulses, known as the input shaper, with a desired reference command. This produces a command that will drive the system while limiting residual vibration [25].

To understand and create a command that can move a system, a simple second-order oscillating system is used. If an impulse is given to any mechanical system, it induces unwanted vibrations in it. This vibration can be cancelled out by applying a second impulse to the system at the right time and the right amplitude, as shown in Figure 38. In Figure 38,

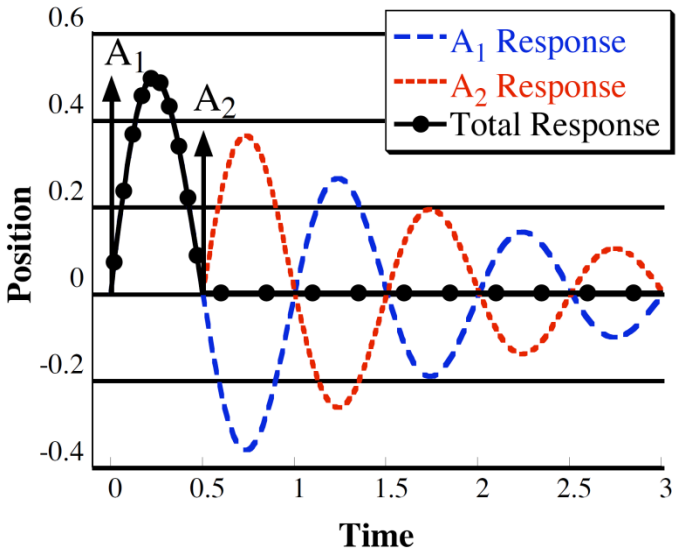

Figure 38. Two Impulse Response [26]

A_1 is the amplitude of first impulse, and A_2 is the amplitude of second impulse applied after the first impulse begins. If the time of second impulse is properly set, the response to it cancels out the oscillations and results in total response, as shown in Figure 38.

A simple second-order under-damped oscillating system equation is:

$$y_0(t) = \left[\frac{A_0\omega}{\sqrt{1-\zeta^2}}\, e^{-\zeta\omega(t-t_0)}\right] \sin\left(\omega\sqrt{1-\zeta^2}(t-t_0)\right) \tag{21}$$

where A_0 is impulse amplitude, t_0 is the time when impulse is applied, ω is the natural frequency and ζ is damping ratio. The response to a sequence of N-impulses after the time of the last impulse is [27]:

$$\sum y(t) = \sum_{i=1}^{n}\left[\frac{A_i\omega}{\sqrt{1-\zeta^2}} e^{-\zeta\omega(t-t_i)}\right] \sin\left(\omega_d(t-t_i)\right) \tag{22}$$

where A_i and t_i are the amplitude and time of i^{th} impulse, n is the total number of impulses and $\omega_d = \omega\sqrt{1-\zeta^2}$. The percentage residual vibration equation resulting from sequence of impulses is given as [27]:

$$V(\omega,\zeta) = e^{-\zeta\omega t_n}\sqrt{[C(\omega,\zeta)]^2 + [S(\omega,\zeta)]^2} \tag{23}$$

where,

$$C(\omega,\zeta) = \sum_{i=1}^{n} A_i e^{\zeta\omega t_i} \cos(\omega_d t_i) \tag{24}$$

$$S(\omega,\zeta) = \sum_{i=1}^{n} A_i e^{\zeta\omega t_i} \sin(\omega_d t_i) \tag{25}$$

To avoid trivial solutions, each impulse amplitude is constrained to be greater than 0

$$\forall A_i \geq 0 \tag{26}$$

and the sum of amplitudes is constrained to one

$$\sum A_i = 1 \tag{27}$$

$$V(\omega,\zeta) = 0 \tag{28}$$

To limit vibration, (23) is set to zero or some small value, as shown in (28). Solving (23) with constraints (26) and (28) gives expressions for amplitudes A_1 and A_2, shown in Figure 38. The constraints are used to minimize the time of the last impulse. The Zero Vibration (ZV) input shaper is [26]:

$$\begin{bmatrix} A_i \\ t_i \end{bmatrix} = \begin{bmatrix} \frac{1}{1+K} & \frac{K}{1+K} \\ 0 & \frac{T_d}{2} \end{bmatrix} \tag{29}$$

where, T_d is the damped oscillation period and the variable K is given as:

$$K = e^{\frac{\zeta\pi}{\sqrt{1-\zeta^2}}} \tag{30}$$

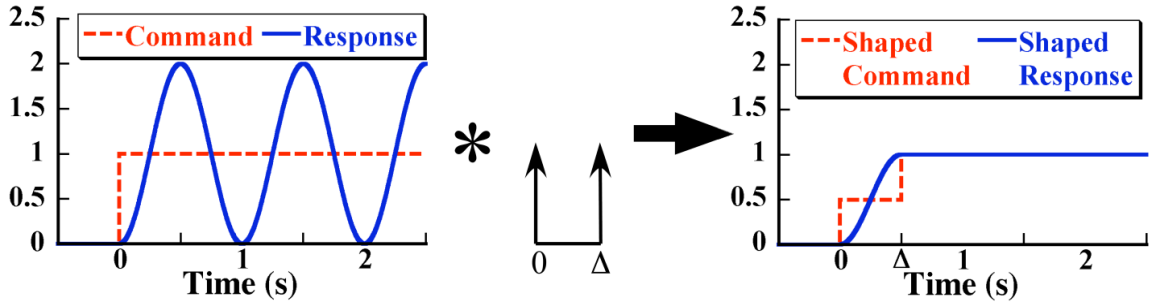

Figure 39. Input Shaping Process [28]

Though this sequence of impulses would reduce vibration, it cannot be used in real systems. A usable command can be generated by convolving the original command with the sequence of impulses. The convolution product of the original command and input shaper is shown in Figure 39. The convolution product forms a shaped command, which will cause the same vibrations as the impulse sequence would. This shaped command can be used to drive a system with very low level of vibrations.

3.1.1 Applications of Input Shaping

Input shaping has been implemented on millions of machines. In systems like cable-driven crane carrying payload, unwanted vibrations are induced due to any input commands. Singer and Seering developed and applied input shaping technique to Draper Laboratory's Space Shuttle Remote Manipulator System Simulator [27]. Yoon, Singhose, and Vaughan applied input shaping technique to crane payloads to reduce bouncing of crane in vertical direction along with payload sway [29]. They showed that input shaping can significantly reduce payload bouncing and sway oscillations using Zero Vibration shaper, shown in Figure 40.

Joel Fortgang, William Singhose, Juan de Marquez, and Jesus Perez applied input shaping technique to micro-mills and CNC controllers, where very high precision is required and even small level of vibration becomes an issue [30].

Freese, Fukushima, Hirose, and Singhose applied input shaping technique to reduce the unwanted oscillations of a long robotic arm used to scan for land mines [31]. Unwanted oscillation for this application corrupts the scanning information, resulting in false alarms. They successfully reduced vibrations in this robotic arm. Karajgikar, Vaughan and Singhose compared the results of PD feedback control and input shaping technique applied to double-pendulum crane operator performance [32]. In this study, they used ten novice crane operators and concluded that input shaping technique helped reduce vibrations significantly and allowed them to complete the positioning task more quickly. Figure 41 shows how input shaping reduced oscillations of the crane hook.

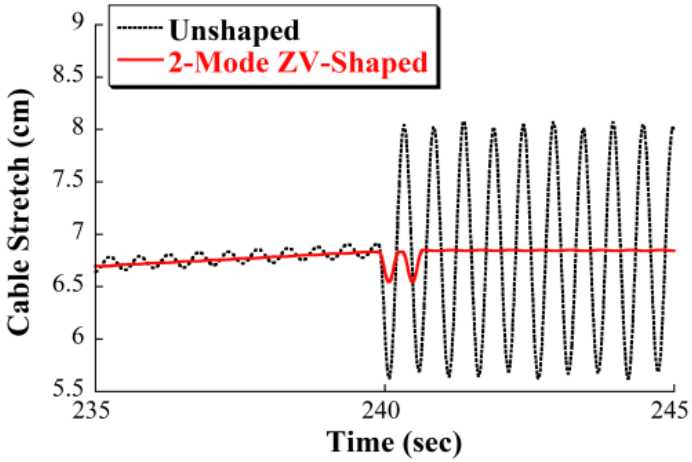

Figure 40. Unshaped and Two-Mode ZV-Shaped Response [29]

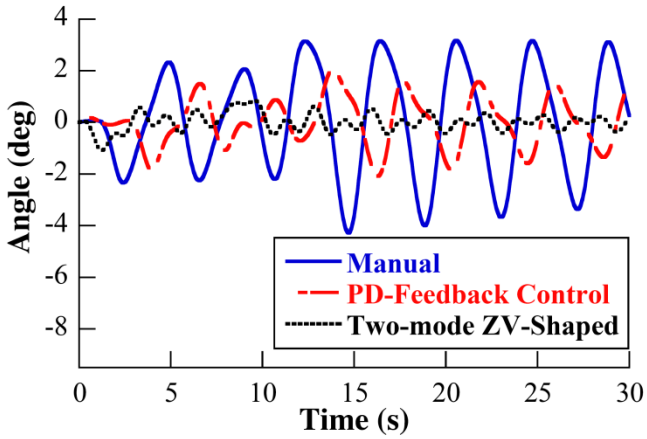

Figure 41. Crane Hook Angle [32]

Huey and Singhose showed that input shaping can be used to significantly reduce vibration in wire-driven mechanisms [33]. Kim and Singhose evaluated input shaping control method for reducing double-pendulum effect of crane payloads [34]. They aimed to carry a payload from start to goal with minimum oscillations possible and in as little time as possible. Figure 42 shows how input shaped command helped reduce significantly payload oscillations of a double pendulum crane.

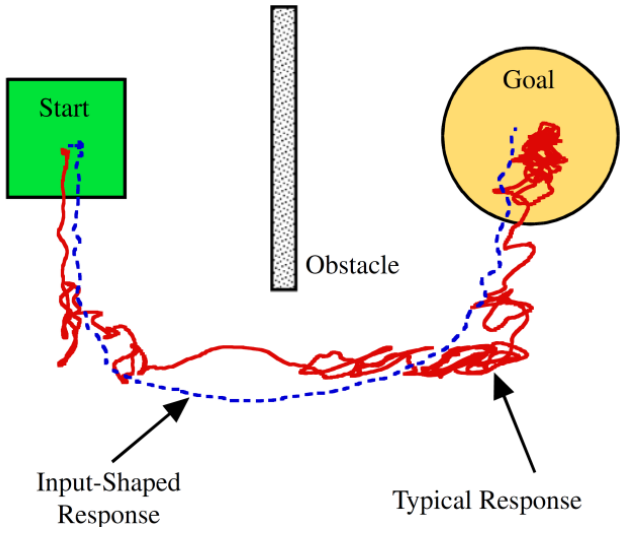

Figure 42. Double Pendulum Hook Response [34]

Blackburn used command shaping to electrodynamics tethers propulsive actuators for orbit boost and station keeping [28]. He developed an intelligent command shaping algorithm that significantly reduced the amount of string vibration.

3.2 System model

Input shaping is an appropriate solution for controlling unwanted oscillations of HiBot's Expliner robot [19]. The parts of Expliner are labeled in Figure 43. As Expliner travels along the cable it encounters obstacles like cable spacers, hangers or clamp suspenders and to traverse these obstacles, Expliner goes into the acrobatic mode, shown in Figure 44, which consists of various steps.

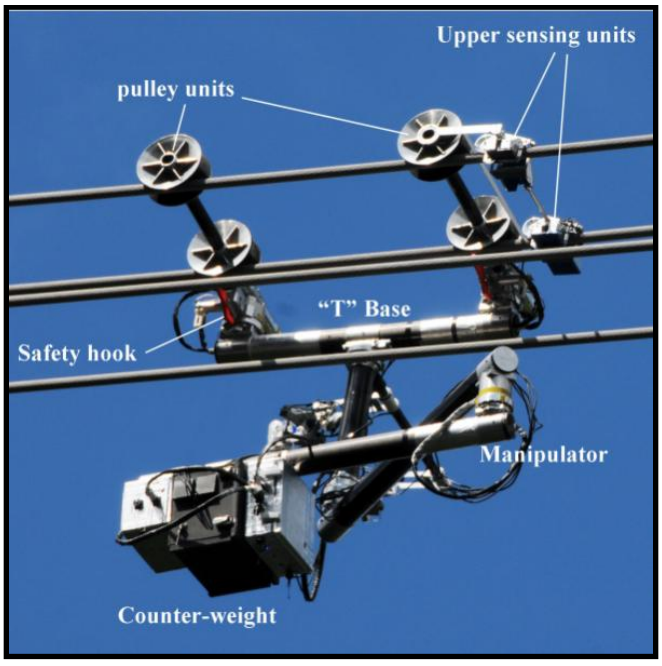

Figure 43. HiBot's Expliner Robot [19]

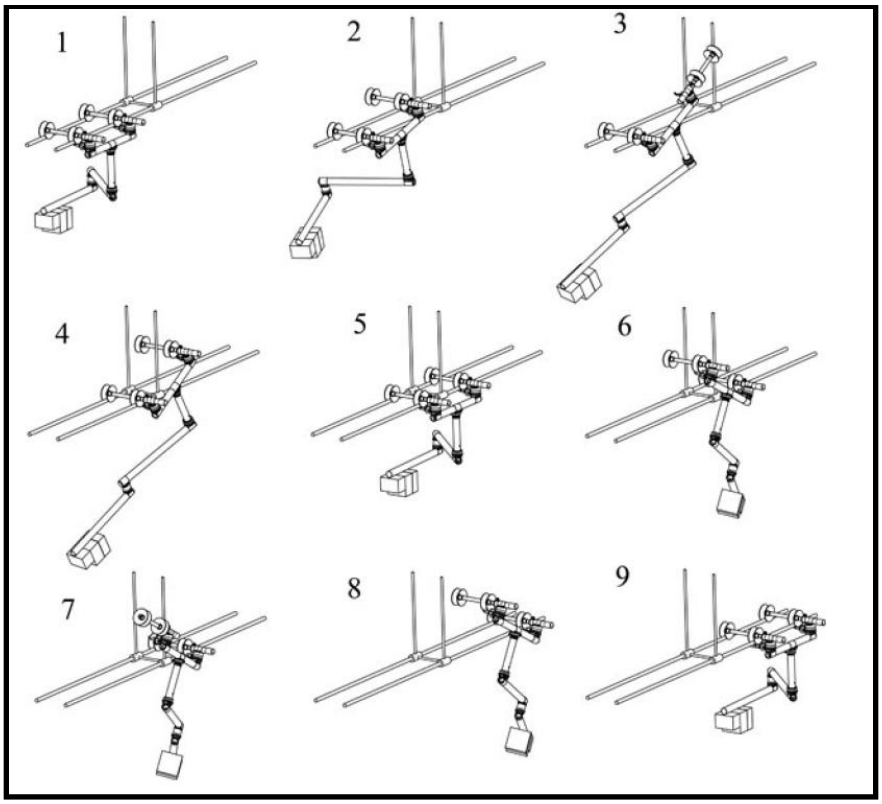

Figure 44. Sequence of Motion of Expliner Robot Overcoming Clamp Suspender [20]

At step 1, Expliner is riding on cable on all 4 pulleys. As Expliner approaches clamp suspenders and enters into the acrobatic mode, the manipulator stretches counter-weight rearwards to shift center of gravity of robot. The counter-weight shifts rearwards until front pulley units lift high enough that they are off the cables and entire robot balances on rear pulley unit like shown in Figure 44 at step 2. The front pulley unit then rotates, out of the way of suspended clamps as shown at step 3, the robot can then move forward on cable on rear pulley unit clearing its way through first half portion of robot as shown at step 4. The counter-weight then moves forward again, shifting the center of gravity, which brings the front pulley down and back on cable as shown at step 5. The manipulator then stretches counter-weight even further until rear pulley units lift up and clear of cables and swaying around out of the way of clamp suspenders. The robot then moves forward on front pulley

units clearing the other portion of robot across the clamp suspender and again shifts counter-weight rearward lowering rear pulley units back onto cable. During the acrobatic mode from step 2 to 4 and step 6 to 8, Expliner travels only on a single pair of pulley units. Expliner is prone to oscillations during these steps. Unwanted oscillations may lead to collision of robot with suspender clamps and can decrease the safety of operation.

For further reference in this chapter, the phases of acrobatic mode are named specifically according to their actions performed as shown in Table 6.

Figure 45 shows the planar model of Expliner during its riding phase, where the circle is the pulley units that ride along cable, m_t is the mass of pulley units away from cable, links of length l_{low} and l_{up} are the manipulator that shifts the counterweight of mass m_{act} forward or rearward. Rocking oscillations are induced in Expliner during riding phase. This planar model is used to determine the natural rocking frequency.

In Figure 45, planar model of Expliner shows two masses, m_t and m_{act}, connected by rigid massless links. These links pivot on pulley units that are riding on cable. Mass m_t is offset from centre on link of length l_{up}. Counter-weight or mass m_{act} is vertically offset

Table 6: Acrobatic Mode Phase Description

Between steps	Called as	Action performed
1 and 3	Transition phase	Counter-weight shifts rearwards to lift front pulley units. Expliner is balancing on rear pulley units
3 and 4	Riding phase	Expliner travels along the cable balancing only on rear pulley units
4 and 5	Lowering phase	Counter-weight shifts forward to lower front pulley units for all pulley units to be on cable

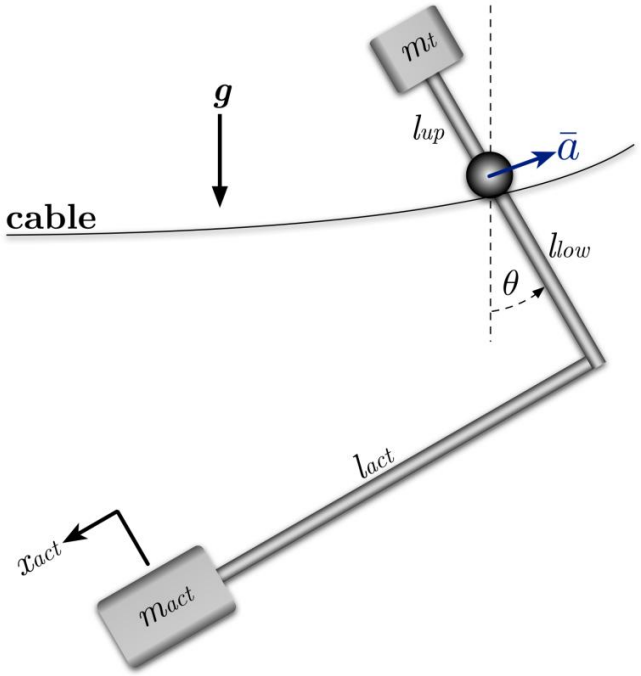

Figure 45. Planar Model of Expliner Moving Along Cable [35]

from center by link of length l_{low} and horizontally by link of length l_{act}. Position of mass m_{act} can change along link of length l_{act} and is determined by $\ddot{x}_{act}$. Expliner's pulleys are equipped with motors that control its speed and acceleration. The inputs to the system are the acceleration of the pulley units along the cable, $\bar{a}$, and the acceleration of the counter-weight.

The equation of motion of Expliner is:

$$\begin{aligned} I_0\ddot{\theta} \;=\; & m_t g l_{up}\sin(\theta) + m_t l_{up}[\cos(\theta)\ddot{x} + \sin(\theta)\ddot{y}] \\ & - m_{act} g[l_{low}\sin(\theta) - l_{act}\cos(\theta)] \\ & - m_{act}\big[(l_{low}\sin(\theta) - l_{act}\cos(\theta))\ddot{y} \\ & + (l_{act}\sin(\theta) + l_{low}\cos(\theta))\ddot{x} + 2l_{act}\dot{\theta}\dot{x}_{act} \\ & - l_{low}\ddot{x}_{act}\big] \end{aligned} \tag{31}$$

where g is acceleration due to gravity, $\ddot{x}$ and $\ddot{y}$ are the horizontal, and vertical components of acceleration $\bar{a}$. $\ddot{x}$ and $\ddot{y}$ are required to be in absolute Cartesian co-ordinates. I_0 is the moment of inertia about the pivot point of robot pulley unit riding on cable.

$$I_0 = m_t {l_{up}}^2 + m_{act}({l_{low}}^2 + {l_{act}}^2) \tag{32}$$

The equilibrium angle, θ_{eq}, is:

$$\theta_{eq} = \tan^{-1}\left(\frac{-l_{act}}{Rl_{up} - l_{low}}\right) \tag{33}$$

where,

$$R = \frac{m_t}{m_{act}} \tag{34}$$

In (31), equations were developed further for $\ddot{x}$ and $\ddot{y}$. The $\ddot{x}$ and $\ddot{y}$ are the absolute Cartesian co-ordinates. Since Expliner travels along a curved path which is catenary curve by nature, equations were initially developed in path co-ordinates. To convert the path co-ordinates to absolute Cartesian co-ordinates, that is the horizontal and vertical acceleration ($\ddot{x}$ and $\ddot{y}$) component of Expliner model, a detailed vector diagram of pulley units riding on cable in riding phase is shown in Figure 46 where e_n, e_t, i, and j are unit vectors. e_n and e_t are perpendicular to each other and i and j are perpendicular to each other. $\bar{a}$ is the input acceleration along unit vector e_t.

Again, $\bar{a}$ is the primary input of Expliner moving along the cable. Absolute acceleration of system is then:

$$\overrightarrow{acc} = \bar{a}e_t + \frac{v^2}{\rho}e_n \tag{35}$$

where ρ is radius of curvature and v is velocity in direction of unit vector e_t

The radius of curvature of the cable, ρ, is:

$$\rho = \frac{\left[1+\frac{dy}{dx}^2\right]^{3/2}}{\frac{d^2y}{dx^2}} \tag{36}$$

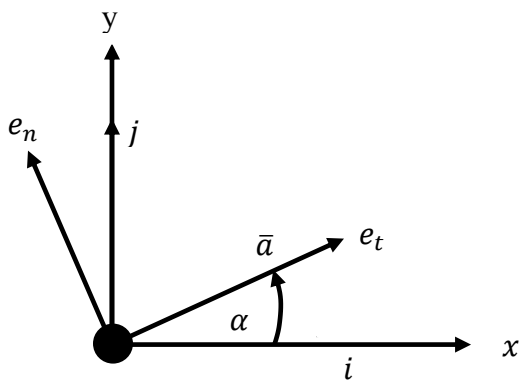

Figure 46. Acceleration Vector Diagram

where y is the path equation of catenary:

$$y = \text{acosh}\left(\frac{x}{a} - b\right) + c \tag{37}$$

Combining (36) and (37), the radius of curvature of the cable as a function of position along it, x, can be written as:

$$\rho = a\frac{\left[1 + sinh\left(\frac{x}{a} - b\right)^2\right]^{3/2}}{cosh\left(\frac{x}{a} - b\right)} \tag{38}$$

This allows the absolute acceleration of the pulley unit to be written as:

$$\overrightarrow{acc} = \bar{a}e_t + \frac{v^2 cosh\left(\frac{x}{a} - b\right)}{a\left[1 + sinh\left(\frac{x}{a} - b\right)^2\right]^{3/2}} e_n \tag{39}$$

$$e_t = (cos\theta i + sin\theta j)$$

$$e_n = (sin\theta i + cos\theta j) \tag{40}$$

Finally, this acceleration can be expressed in Cartesian co-ordinates:

$$\therefore \overrightarrow{acc} = \left(\bar{a}cos\theta + \frac{v^2 cosh\left(\frac{x}{a} - b\right)}{a\left[1 + sinh\left(\frac{x}{a} - b\right)^2\right]^{3/2}} sin\theta \right) i + \left(\bar{a}sin\theta + \frac{v^2 cosh\left(\frac{x}{a} - b\right)}{a\left[1 + sinh\left(\frac{x}{a} - b\right)^2\right]^{3/2}} cos\theta \right) j \quad (41)$$

The horizontal and vertical components of input acceleration $\vec{a}$ can be written as:

$$\overrightarrow{acc} = \ddot{x}i + \ddot{y}j \quad (42)$$

$$\ddot{x} = \left(\bar{a}cos\theta + \frac{v^2 cosh\left(\frac{x}{a} - b\right)}{a\left[1 + sinh\left(\frac{x}{a} - b\right)^2\right]^{3/2}} sin\theta \right) \quad (43)$$

$$\ddot{y} = \left(\bar{a}sin\theta + \frac{v^2 cosh\left(\frac{x}{a} - b\right)}{a\left[1 + sinh\left(\frac{x}{a} - b\right)^2\right]^{3/2}} cos\theta \right) \quad (44)$$

Equations (43) and (44) can then be used in (31) to simulate the response of the Expliner.

3.3 Rocking Oscillation of Expliner

Rocking oscillations are induced in Expliner during the riding phase of its acrobatic mode. To investigate the transient and residual oscillation vibration of the system, parameters used for Expliner simulation are given in Table 7. The configuration shown in Table 7 results in a natural frequency of $0.47Hz$. This frequency is used to design an input shaper.

Parameters l_{low}, l_{up}, l_{act}, m_t, and m_{act} in Table 7 are labeled in Figure 45.

Parameter $|\bar{a}_{\max}|$ is the maximum acceleration of input command, $|\bar{v}_{\max}|$ is the maximum

Table 7: Expliner Simulation Parameters

Parameter	Value
l_{low}	$0.75m$
l_{up}	$0.125m$
l_{act}	$0.75m$
$\lvert\bar{a}_{max}\rvert$	$1\,m/s^2$
$\lvert\bar{v}_{max}\rvert$	$0.3\,m/s$
m_t	$10kg$
m_{act}	$25kg$
Move distance	$3m$
Cable length	$274m$
Cable Sag	$9.7m$

velocity with which Expliner can travel, and move distance is the distance traveled during riding phase. Cable length is the total length of high-voltage power transmission overhead cable in between spans, and sag is the deviation of centre of simply supported cable from supports which defines the catenary curve.

With values of $|\bar{a}_{\max}|$, $|\bar{v}_{\max}|$, and move distance, a bang-coast-bang input acceleration command was generated, shown in Figure 47. This command is also called as the unshaped or reference command. Figure 48 shows the velocity resulting from input acceleration command, which gives a clear idea of velocity with which Expliner rides along the cable.

Since Expliner is traveling along curved cable the input acceleration is resolved into horizontal and vertical component. Figure 49 shows horizontal component of input acceleration, while Figure 50 shows vertical component of input acceleration. From Figures 49 and 50, it is observed that horizontal component of acceleration is much greater than vertical component. This is expected given the relatively low radius of curvature of the cable on which Expliner is riding.

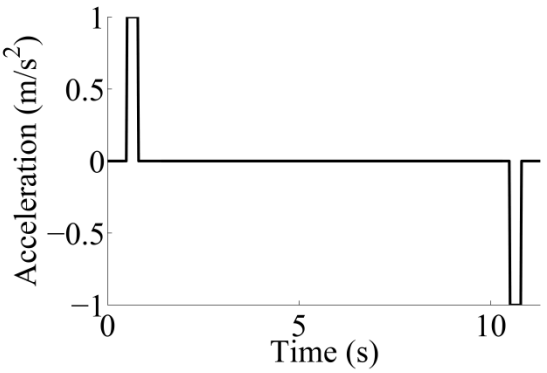

Figure 47. Unshaped Acceleration Input

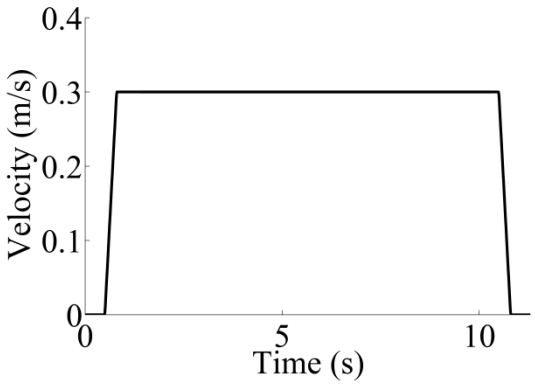

Figure 48. Velocity Command

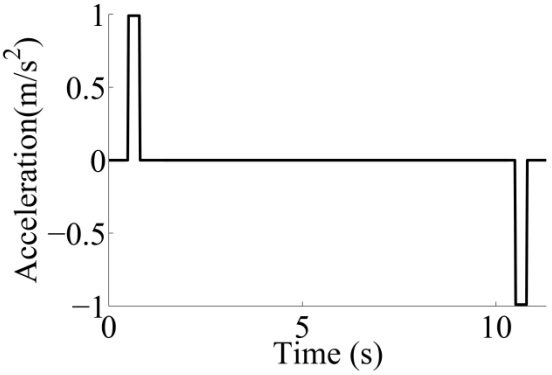

Figure 49. ($\ddot{x}$), Horizontal Component of Input Acceleration

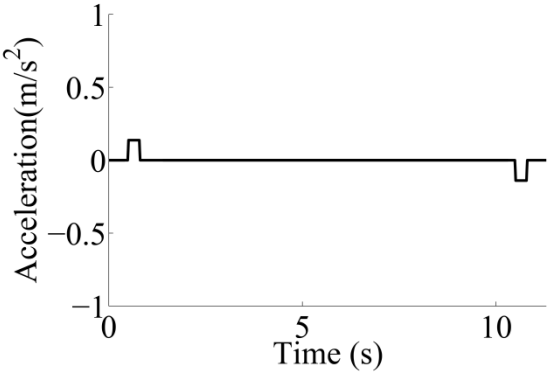

Figure 50. ($\ddot{y}$), Vertical Component of Input Acceleration

The unshaped acceleration input command results in rocking transient as well as residual oscillations, as shown in Figure 51. Figure 51 is a plot of time versus the oscillation angle. The deviation of the link of length l_{up} from vertical is the angle plotted in Figure 51, which is the oscillation angle. The y-axis, angle, in Figure 51 is labeled as θ in Figure 45. These rocking oscillations can cause problems in safety of inspecting of cables during riding phase. The on-board cameras and sensors can smash against the cable or suspended clamps.

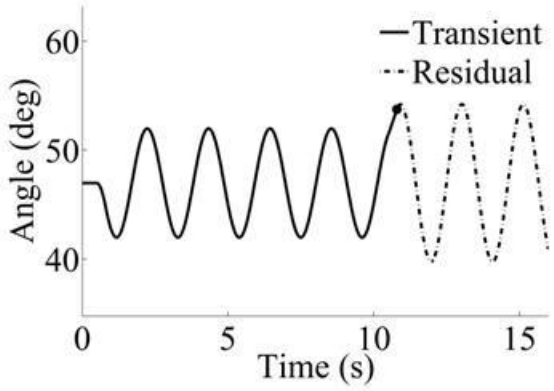

Figure 51. Unshaped Rocking Oscillation for Move Distance $3m$

3.4 Using Shaped Command to Reduce Rocking Oscillations

Input shaping was used to reduce rocking oscillations. For parameters given in Table 6, frequency $0.47Hz$, a zero-vibration input shaper was developed from (29):

$$ZV \equiv \begin{bmatrix} A_i \\ t_i \end{bmatrix} = \begin{bmatrix} 0.5 & 0.5 \\ 0 & 1.05 \end{bmatrix} \tag{45}$$

This input shaper which is two impulses cannot be used to drive the mechanical system. This input shaper is convolved with the unshaped or reference input command to get the shaped command shown in Figure 52 and 53. This product of convolution resulting in shaped command is used to drive the system.

Figure 53 shows response of system created by acceleration input command $\bar{a}$ and Zero Vibration (ZV) shaped response of the same system for same parameters. Figure 54 shows that transient as well as residual vibrations of unshaped response are reduced significantly using shaped command. The acceleration input command stops at approximately $11s$, where the transient vibrations end and the residual vibrations begin for unshaped response. The shaped command stops at approximately $12s$.

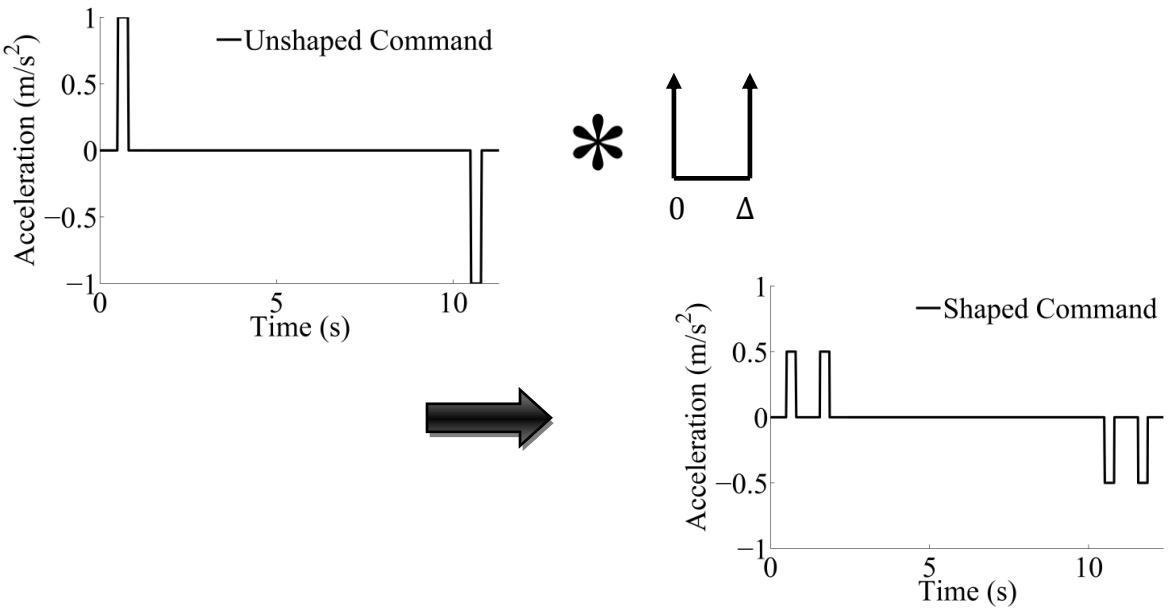

Figure 52. Input Shaping Process for Acceleration, for Parameters given in Table 5.

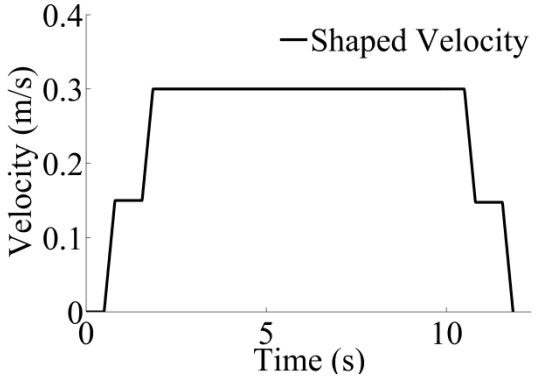

Figure 53. Shaped Velocity

While the ZV shaped command reduced the transient as well as residual vibration, the time of input command increased by approximately $1s$ $(12s - 11s)$. This delay of 1s is a penalty for dramatic reduction in vibration.

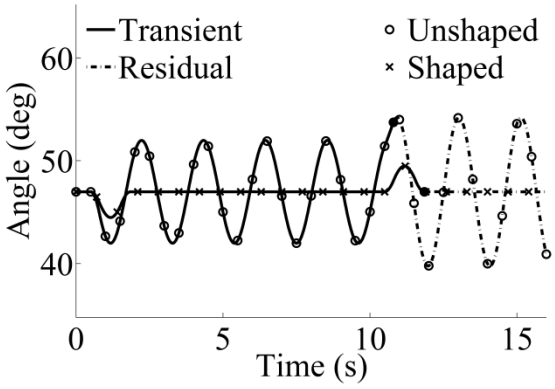

Figure 54. Unshaped and ZV-Shaped Rocking Oscillation

3.4.1 Analysis of Rocking Oscillation during Riding Phase

To investigate if such low level oscillation can be achieved using input shaping for varying move distance, simulations were run for same set of parameters given in Table 7, but varying move distance. Expliner was made to travel with move distance between $2m$ and $3.5m$ from the end of cable to the clamp. The reason for limiting move distance to at least $2m$ or greater is the total length of Expliner which is about 1.5m. The width of Expliner is about $0.5m$, which is the distance between two pulleys of same unit. During transition phase, the front pulley units rotate around to avoid collision of front pulleys with the suspender clamps. As a result, Expliner has to start its transition phase approximately $1.5m + 0.5m$ away from the clamp. Figure 55, and Figure 56 shows how Expliner motion is simulated with move distances between $2m$ and $3.5m$.

For a move distance of $2m$, a high level of residual vibration for unshaped response is caused by constructive interference, as shown in Figure 57. For move distance $2.52m$, low level of residual vibration is caused by destructive interference, as shown in Figure 58. High level of residual vibration for the unshaped response is shown in Figure 59 for a move distance 2.78m, and a low level of vibration, for unshaped response is again shown in

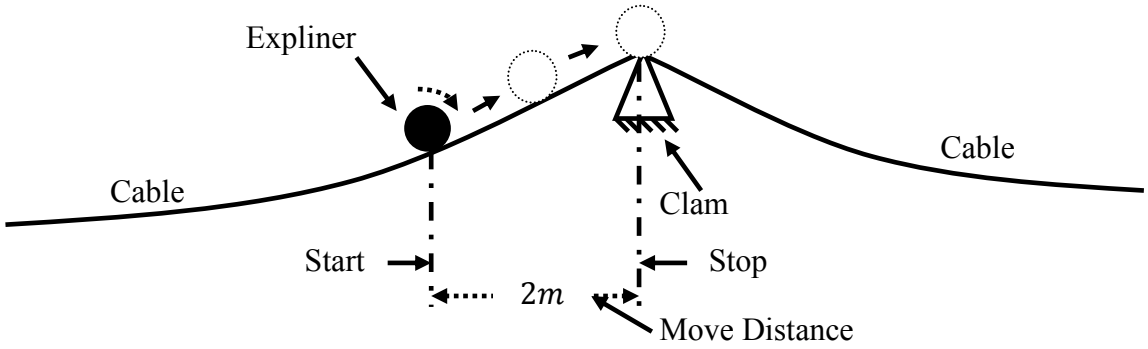

Figure 55. Expliner Starting its Acrobatic Mode from Distance $2m$

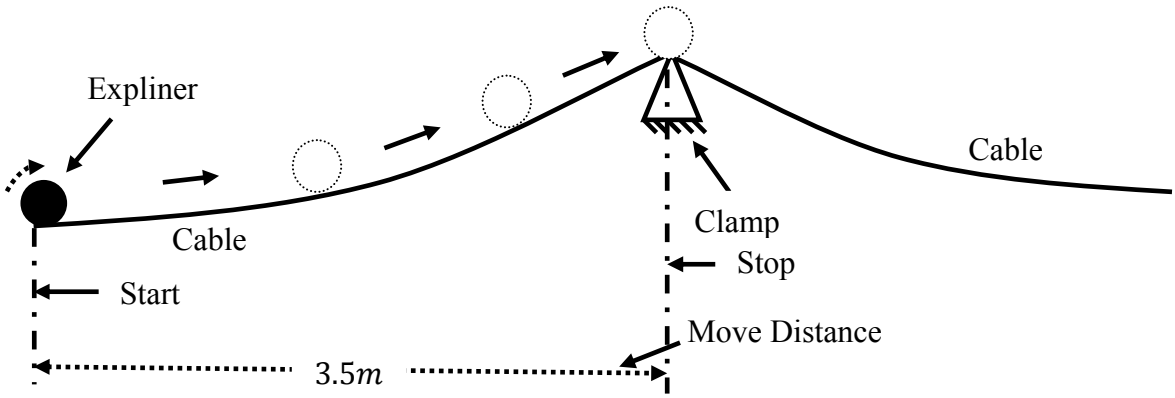

Figure 56. Expliner Starting its Acrobatic Mode from Distance $3.5m$

Figure 60 for a move distance 3.17m. These simulations were run for velocity 0.3m/s. For unshaped moves, the residual unshaped oscillations are a function of move distance.

The shaped response seen in Figure 57 shows no residual vibration. The transient vibration, of amplitude 2 degrees, at 1s and 8s is inevitable. This is a dramatic reduction in the rocking of Expliner. This makes the inspection operation of Expliner safe. Simulations were run for varying move distances, ranging from 2m to 3.5m. Figures 57, 58, 59, and 60 shows the same vibration reduction due to shaped response.

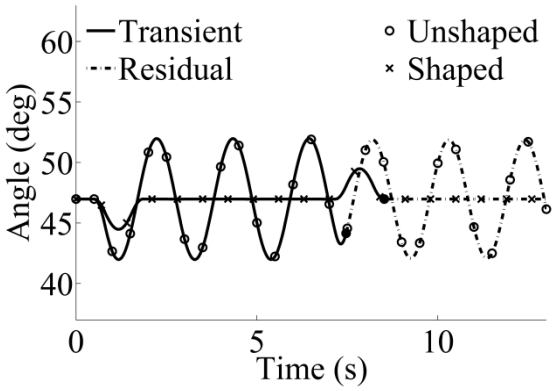

Figure 57. Unshaped and Shaped Rocking Oscillation for Move Distance $2m$

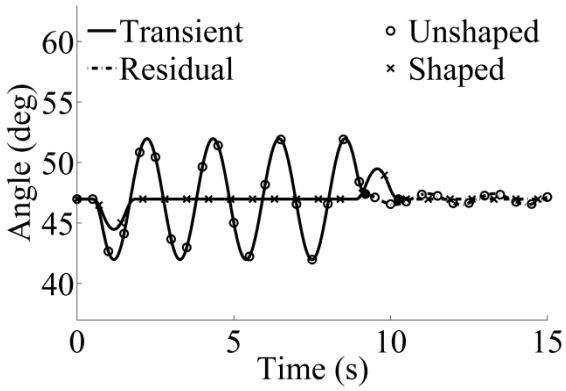

Figure 58. Unshaped and Shaped Rocking Oscillation for Move Distance $2.52m$

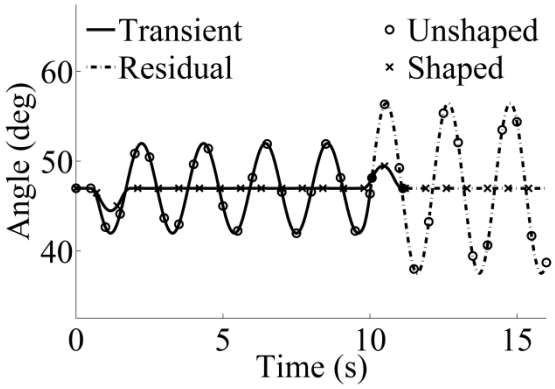

Figure 59. Unshaped and Shaped Rocking Oscillation for Move Distance $2.78m$

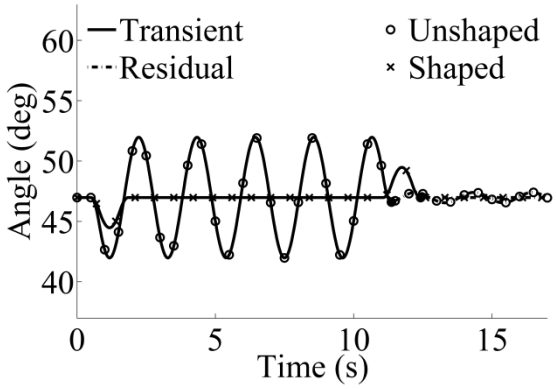

Figure 60. Unshaped and Shaped Rocking Oscillation for Move Distance $3.17m$

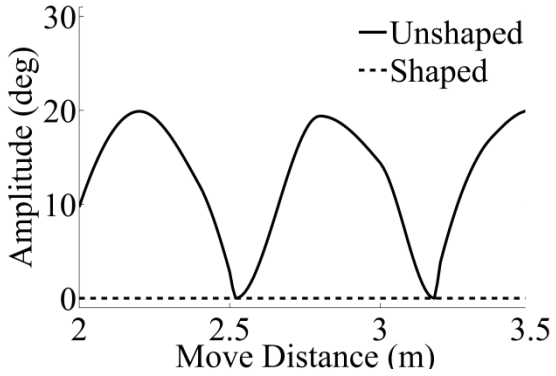

Figure 61. Residual Rocking Amplitude as a Function of Move Distance, for v_{max} $0.3\,m/s$

For different move distances, the amplitude of oscillations varies according to amount of constructive or destructive interference resulting from the acceleration and deceleration portions of point-to-point command [35]. This phenomenon is summarized in Figure 61 for move distances between $2m$ and $3.5m$. In Figure 61, at certain move distances, low levels of residual vibrations are observed, while at some other move distances large amount of oscillations are observed. Yet for any move distance, the shaped command effectively reduced the residual rocking oscillations to zero.

Simulations were also run for varying speeds. The speed of Expliner is constrained due to its design. Expliner can travel with a linear speed between $0.38m/s$ and $0.43m/s$ [20]. Sensors used to inspect cable also is a constraining factor for its speed, which may lower the operation speed below $0.38m/s$. Further development of Expliner may increase its inspection speed to greater than $0.5m/s$. Hence, simulations were also run for velocities $0.4\,m/s$, $0.5\,m/s$ and $0.6\,m/s$. Figures 62, 63, and 64 show the residual amplitude as function of move distance with velocities $0.4\,m/s$, $0.5\,m/s$ and $0.6\,m/s$, respectively. As speed increases, destructive interference takes place at greater interval of move distances.

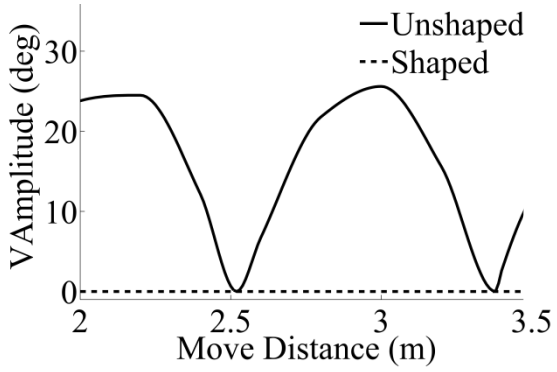

Figure 62. Residual Rocking Amplitude as a Function of Move Distance, for v_{max} $0.4\,m/s$

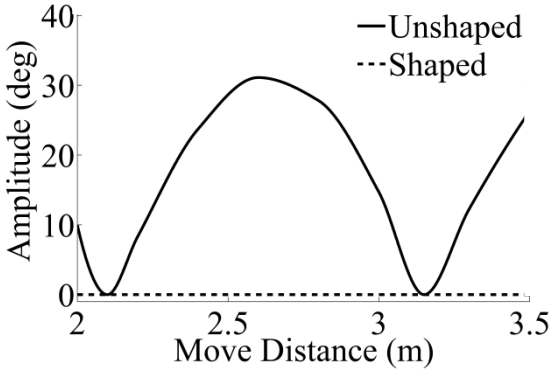

Figure 63. Residual Rocking Amplitude as a Function of Move Distance, for v_{max} $0.5\,m/s$

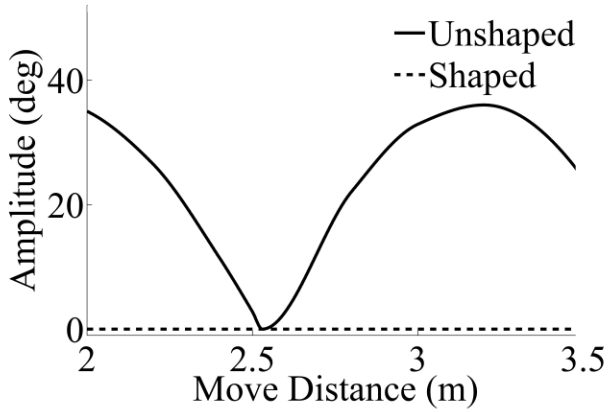

Figure 64. Residual Rocking Amplitude as a Function of Move Distance, for v_{max} $0.6\,m/s$

For any given velocity, it is observed from Figures 62, 63, and 64 that the shaped amplitude is zero. ZV input shaping significantly reduced residual oscillations for any required move distances and any given moving velocity.

Figure 65 shows the unshaped residual vibration amplitude as a function of move distance between $2m$ and $3.5m$ and v_{max} between $0.3\,m/s$ and $0.6\,m/s$. From Figure 66, it was noted that even without using input shaper, for some move distances, residual vibrations can be significantly reduced, but residual oscillations also increases to its peak for certain move distances. It was also noted that residual vibration amplitude increases with increase in maximum velocity. For velocity $0.3m/s$, the vibration amplitude reaches to 20 degrees, while for velocity $0.6m/s$ the vibration amplitude reaches to 39 degrees. Using input shaped command, the residual vibration is zero for all velocities and move distances.

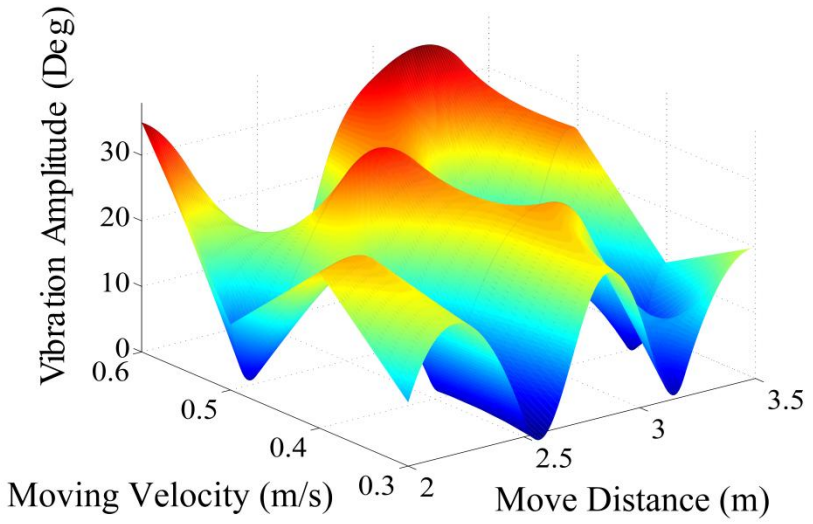

Figure 65. Residual Vibration Amplitude as Function of Move Distance and Velocity

3.4.2 Analysis of rocking oscillations during transition phase

Rocking oscillations may occur during its transition to the acrobatic mode that is the transition phase. These rocking oscillations may cause instability during its transition to the acrobatic mode. Simulations were run for the transition phase and continued to riding phase, since any residual oscillations of transition phase may add to rocking oscillations of riding phase. For the manipulator actuator, which moves the counter-weight mass m_{act}, simulated response is shown in Figure 66 for parameters given in Table 8.

Table 8: Actuator Simulation Parameters

Parameters	Values
Actuator maximum acceleration	$1\,m/s^2$
Actuator maximum velocity	$0.35\,m/s$
Actuator move distance	$0.75m$
Actuator start time	$0s$
Riding start time	$5s$

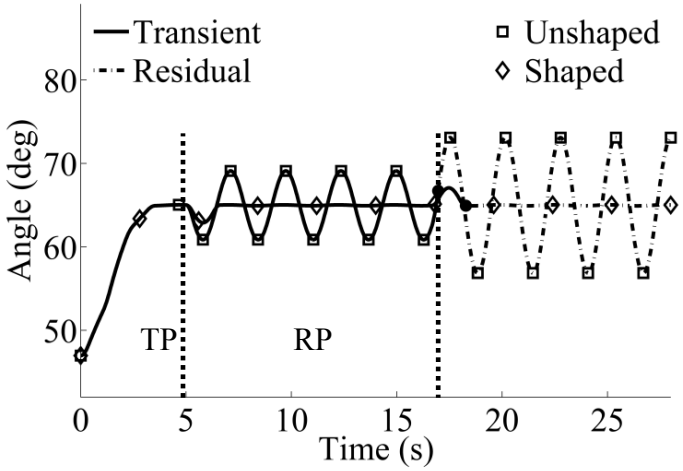

Figure 66. Unshaped and Shaped Response Created During Acrobatic Motion from Transition Phase (TP) to Riding Phase (RP)

In Figure 66, Expliner required about first 5 seconds of total time to complete the transition phase (TP). Riding phase (RP) is completed in the time interval between $5s$ and $17s$, that is when Expliner is riding on cable for a move distance of $3.5m$.

There is a very low level of rocking oscillation and negligible vibration amplitude during transition phase. This oscillation is much lower than that caused during riding phase.

The oscillations from transition phase had almost no effect on oscillations generated during riding phase. Input shaping can still effectively reduce transient as well as residual vibrations from transition phase to riding phase, shown in Figure 66.

3.4.3 Analysis of Rocking Oscillation during Lowering Phase

Rocking oscillations may also cause problems during Expliner's lowering phase, that is when counter-weight moves forward for both pulley units need to be on cable. Simulation of this phase is shown in Figure 67, and very low level of oscillations is observed, which are significantly lower than oscillations during riding. Input shaping works well for given example moves, but to investigate if input shaping can actively reduce residual oscillating

vibrations of Expliner for all possible high voltage power transmission cable length, span and sag, these parameters are altered and simulated. A study is made for 7 different configurations of cable length, span and sag, which are commonly found and reported by IEEE task force [21]. Configurations for cable span and sag used for simulations are shown in Table 9.

Cable length, span, and sag determines the radius of curvature of the path followed by Expliner, and the equation of path plays a major role in dynamics of robot as observed in (31). Hence simulations were run for varying cable span, sag, and velocity. The simulated results are shown in Figure 68, and it was observed that the amplitudes of vibration for unshaped response are greater for all cable spans.

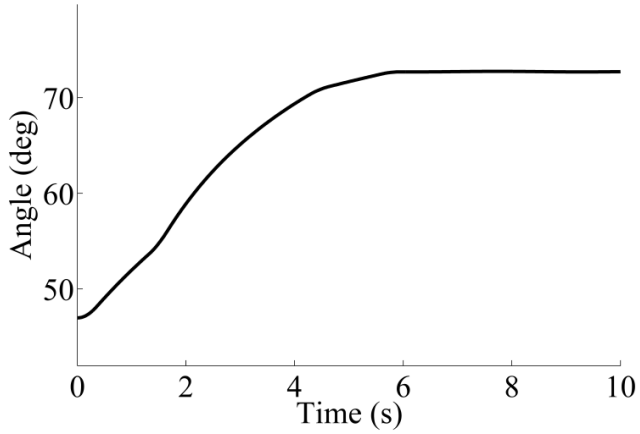

Figure 67. Response Created during Lowering Phase

Table 9: Cable Parameters

	Set 1	**Set 2**	**Set 3**	**Set 4**	**Set 5**	**Set 6**	**Set 7**
Cable span (ft)	450	650	750	850	950	1150	1500
Cable span (m)	137.1	198.1	228.6	259	289.6	350.5	457.2
Cable sag (ft)	8.1	16.2	22.2	26.9	33.4	50.2	78.2
Cable sag (m)	2.5	5	6.8	8.2	10.2	15.3	23.8

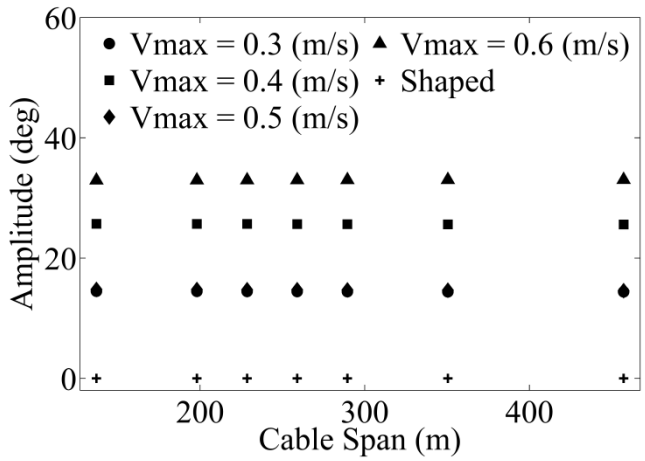

Figure 68. Comparing Unshaped Residual Amplitude with Shaped Residual Amplitude

In Figure 68, Markers ●,■,◆and▲Represent Amplitudes of Unshaped Response, + Represent Amplitude of Shaped Response for All Velocities. It was observed from Figure 68 that input shaping produces zero residual vibration for all given cable span, sag, and for all given velocities.

3.5 Conclusion

In this chapter, an input shaping technique was introduced, which reduces vibrations. Input shaped commands were used to drive Expliner, and very little vibration was noted. Simulations were run for varying Expliner parameters, including velocity, move distance, and varying cable parameters like cable span and sag. For all given changes in parameters, input shaping significantly reduced rocking oscillations.

Chapter IV Conclusions and Future work

Every flexible mechanical system is prone to unwanted vibrations. Suspended cables are used by cable cars for transportation. But, the dynamics of the cables present some limit to the performance of the system. In case of cable cars, it is necessary to maintain safety and reduce unwanted vibrations. It is important to create a control system that can significantly reduce the vibrations in cables. This thesis provided a new, simple cable-mass system that mimics the dynamics of cable, but captures only the dominant dynamic effects. Existing cable models were studied, but with the complex differential equations, it was difficult to develop a control system using these.

In Chapter 2, a simple two spring-mass model was developed and the response from this model was compared to the response from the beam model. It was shown that the two spring-mass model closely matches the beam model. This two spring-mass model can be used to simulate the response. This new model is easy and simple to use and can be applied to various fields where dynamic response of cable needs to be determined. A maximum percentage root-mean-square-error of 0.46% between the two spring-mass model and the beam model was observed. This error is negligible for this application. Thus, a new, and simple cable model was successfully developed.

Since the new developed model is a simple spring-mass system, an efficient control system can be designed to reduce the cable vibrations due to moving load. But it was noted that, for Expliner weighing only 90kg, little vibration was observed near the end of the cable. Hence, a control system was developed for this application. Even though this cable vibration

does not affect the inspection operation of Expliner, rocking oscillations are induced in it due to its travel on cable.

Chapter 3 derived the dynamics of Expliner and a planar model was developed. Simulations were run of Expliner riding along the cable, and the residual rocking oscillation with amplitude as high as 39 degrees were noted. This rocking oscillation was reduced to 2 degrees using input shaper. Input shaping is easy to implement and it offers a simple solution for vibration reduction, since only a few parameters are required to design an input shaper. The simulations run were for the Expliner traveling along a curved catenary path, formed by the suspended power transmission cable. Input shaping was able to reduce oscillation significantly, even on curved paths.

4.1 Future Work

The work presented in Chapter 2 can be used for future analysis of dynamics of wire driven systems. The new simpler two spring-mass model can be used for investigating vibrations in a cable car system. With this simple model a control system can be created to reduce cable vibrations. Expliner weighed only about 90kg, hence the cable vibrations did not affect its inspection operation. However, for further development, Expliner can carry out the maintenance task along with inspection. The retro-fits added to Expliner to carry out maintenance task may lead to increase in the total mass of the robot. The two spring-mass model can then be used to simulate the dynamic response and with increase in weight, the vibration amplitude may increase. A control system can be developed in future work, to reduce this vibration using this simple model.

In Chapter 3, Zero Vibration (ZV) input shaper significantly reduced the rocking oscillation of Expliner. There exist other input shapers that can be used in future work. These shapers can be advantageous if the exact frequency of the system is difficult to determine. Comparison can be made between the shapers by using them to run simulations of Expliner.

In further development of Expliner, the speed of expliner inspection operation may be increased to more than 0.43m/s. If Zero Vibration shaper cannot significantly reduce the rocking oscillations for higher velocities, other known shapers or new shapers developed can be used.

Input shaping technique can be applied to HiBot's Expliner robot to reduce its rocking oscillations. An input shaper can be developed that will create a shaped command which will be used to drive the system. Input shaping parameter, frequency, can be obtained easily with the help of planar model or by experiment. Other parameter, the damping, can be found experimentally. With help of these parameters, a robust input shaper can be developed.

REFERENCES

[1] Niewiroski, Rich Jr. *Golden Gate Bridge.* 2007. Photograph. http://en.wikipedia.org/, San Francisco. Web. 8 Sep 2013.

[2] *First 10-seater monocable gondola lift*. 2010. Photograph. http://en.leitner-ropeways.com, Kronplatz. Web.

[3] Edward S. Neumann, "Cable Propelled Systems in Urban Environments," Retrieved on 2010-08-05.

[4] *The first four normal modes of vibration of a string fixed at each end.* 2012. Photograph. http://projects.kmi.open.ac.uk/Web. 11 April 2012.

[5] Yi-Ming Wang, "The transient dynamics of a cable-mass system due to the motion of an attached accelerating mass," *International Journal of Solids and Structures, Volume 37, Issue 9*, February 2000, Pages 1361-1383, ISSN 0020-7683.

[6] Knawa, M. and Bryja, D., "Nonlinear vibrations of a ropeway system with moving passenger cabins," *Proc. Appl. Math. Mech.*, (2007), 7: 4040045–4040046.

[7] James M.W. Brownjohn, "Dynamics of an aerial cableway system, Engineering Structures," *Volume 20, Issue 9*, September 1998, Pages 826-836, ISSN 0141-0296.

[8] Wu, J.-S. and Chen, C.-C., "The dynamic analysis of a suspended cable due to a moving load," *Int. J. Numer. Meth. Engng*., 28: 2361–2381. (1989).

[9] W. W. Recker, J. Acoust, "Asymptotic Dynamic Response of a Taut String on an Elastic Foundation to a Randomly Moving Load," *Soc. Am*. 48,313 (1970).

[10] Manuel Ferretti, Giuseppe Piccardo, "Dynamic modeling of taut strings carrying a traveling mass," *Continuum Mechanics and Thermodynamics March 2013, Volume 25*, Issue 2-4, pp 469-488.

[11] Metrikine, A.V, Bosch, A.L.,"Dynamic response of a two-level catenary to a moving load," Journal *of Sound and Vibration, Volume 292 (3) Elsevier*- May9, 2006.

[12] V. Zoller, I. Zobory, "Relations Between the Motion-Responses Caused by Fixed and Moving Loads Acting on Discretely Supported Strings and Beams," *Progress in Industrial Mathematics at ECMI 2000 Mathematics in Industry Volume 1, 2002*, pp 657-661.

[13] Kristina Hamachi LaCommare and Joseph H. Eto, "Understanding the Cost of Power Interruptions to U.S. Electricity Consumers," *Environmental Energy Technologies Division September 2004* < http://eetd.lbl.gov/ea/EMP/EMP-pubs.html>.

[14] *Eastern Alberta Transmission Line project.* 2013. Photograph. FreeDigitalPhotos.net, Alberta. Web. 12 March 2013.

[15] *All Aluminium Conductor Overhead Cable.* 2012. Photograph. http://zzhlcable.en.made-in-china.com, China. Web.

[16] *Straight Up: Helicopters in Action* Video by IMAX. (January 1, 2002) < http://www.youtube.com/watch?v=Oy81YP-q8R4>.

[17] Xiaohui Xiao, Gongping Wu, Hua Xiao and Jinchun Dai, "An Inspection Robot for High Voltage Power Transmission Line and Its Dynamics Study," *Service Robot Applications, Yoshihiko Takahashi (Ed.), ISBN: 978-953-7619-00-8, (2008) InTech*.

[18] Serge Montambault and Nicolas Pouliot, "Design and Validation of a Mobile Robot for Power Line Inspection and Maintenance," *6th International Conference on Field and Service Robotics - FSR 2007.*

[19] www.hibot.co.jp by HiBot Corp., Expliner Pamphlet.

[20] Paulo Debenest, Michele Guarnieri et al. "Expliner–Toward a Practical Robot for Inspection of High-Voltage Lines," *HiBot Corp., Tokyo Institute of Technology, Kansai Electric Power Corp., J-Power Systems Corp., Kanden Engineering.*

[21] Mehran Keshavarzian and Charles H. Priebe, "Sag and Tension Calculations for Overhead Transmission Lines at High Temperatures-Modified Ruling Span Method*," IEEE Transactions on Power Delivery, Vol. 15, No. 2, April 2000.*

[22] Ladislav Frýba, "Vibration of solids and structures under moving loads," *Monographs and textbooks on mechanics solids and fluids / Mechanics of structural systems Volume 1 1972.*

[23] Graff, Karl F., "Wave motion in elastic solids," *Ohio State University Press* (1975).

[24] Apaydin. A., "Moving loads on elastically supported beams," *Ph.D thesis, Virginia tech* (1978).

[25] Smith, O. J. M., "Feedback Control Systems," *New York: McGraw-Hill Book Company, Inc., 1958,* pp. 331–345.

[26] William Singhose, "Command Shaping for Flexible Systems: A Review of the First 50 Years," *International Journal of Precision Engineering and Manufacturing Vol. 10,* No. 4, pp. 153-168.

[27] N. C. Singer and W. P. Seering, "Preshaping command inputs to reduce system vibration," *Journal of Dynamic Systems, Measurement, and Control, vol. 112*, pp. 76 - 82, March 1990.

[28] David F. Blackburn "Command Shaping for Vibration Reduction in Nonlinear Cabled Systems" *George W. Woodruff School of Mechanical Engineering Georgia Institute of Technology*, August 2006.

[29] Yoon, J.; Nation, S.; Singhose, W.; Vaughan, J.E., "Control of Crane Payloads That Bounce During Hoisting," *Control Systems Technology, IEEE Transactions on*, vol. PP, no.99, pp.1,1, 0

[30] Joel Fortgang, William Singhose, Juan de Juanes M´arquez, Jesus P´erez, "Command Shaping for Micro-Mills and CNC Controllers," *American Control Conference* June 8-10, 2005.

[31] M. Freese, E. F. Fukushima, S. Hirose, and W. Singhose, "Endpoint vibration control of a mobile endpoint vibration control of a mobile mine-detecting robotic manipulator," *in Proceedings of 2007 American Control Conference*, New York, NY, United states, 2007, pp. 7 -12.

[32] Ajeya Karajgikar, Joshua Vaughan and William Singhose, "Double-pendulum crane operator performance comparing PD- feedback control and input shaping," *Advances in Computational Multibody Dynamics 2011, ECCOMAS Thematic Conference Brussels*, Belgium, 4-7 July 2011.

[33] John Huey and William Singhose "The application of input shaping to wire-driven mechanisms," *The 6th international conference on motion and vibration control, Saitama*, August 19-23, 2002.

[34] D. Kim and W. Singhose, "Performance studies of human operators driving double-pendulum bridge cranes," *Control Engineering Practice, vol. 18*, no. 6, pp. 567 - 576, 2010.

[35] Joshua Vaughan, “Modeling and control of rocking in cable-riding systems,” in 2013 *Asian Control Conference (ASCC),* June 2013.

Dhundur, Ninad Pravin. Bachelor of Engineering, Mechanical Engineering, University of Mumbai, Spring 2011; Master of Science, Engineering, Mechanical Engineering option, University of Louisiana, Fall 2013
Major: Engineering, Mechanical Engineering option
Title of Thesis: Modeling and Control of Cable-Riding Robots
Thesis Director: Dr. Joshua Vaughan
Pages in Thesis: 76; Words in Abstract: 265

ABSTARCT

Cables are used in various fields like construction, sports, communication, and transportation. Two important fields where cables are used for this research are transportation and high-voltage power lines. In the field of transportation, cables are used in cable-riding systems like cable cars, tramways, and gondola lifts. Vibration is induced in these systems. These vibrations are undesirable.

High-voltage power line cables are important part of our lives. Inspection of these power lines is necessary to eliminate the risk of power outages. Earlier power lines were inspected by skilled humans by crawling along the power lines. This inspection task was replaced by cable riding inspection robots to eliminate the risk to human life.

This research explains various inspection robots and problems in these types of cable-riding systems. In this research, to determine the vibrations in the cable due to riding load, a new simple cable-mass system was developed. This new cable-mass system makes it easy to develop a control system to reduce the cable vibrations.

To inspect the power lines, HiBot developed an inspection robot called Expliner that travels along the live power lines. For uninterrupted inspection operation, Expliner traverses obstacles on the power lines with its intelligent acrobatic mode. In this mode, Expliner is subjected to rocking oscillation. This rocking oscillation is also induced in the cables cars. This rocking is undesirable and is unsafe.

This research introduces a method to reduce rocking in cable-riding systems. This method, called input shaping, is used to run simulations for Expliner traveling along curved cables. This research develops an input shaper to reduce rocking in cable-riding robots like Expliner.

BIOGRAPHICAL SKETCH

Ninad Dhundur grew up in Mumbai, India. With the support of his parents, Mr. Pravin Dhundur and Mrs. Priyali Dhundur, he attended the University of Mumbai where he earned Bachelor of Engineering, Mechanical Engineering. With the support of his parents he attended University of Louisiana at Lafayette where he earned his Master of Science degree in Engineering, Mechanical Engineering option. In this program, he successfully completed his master's thesis with the help of thesis director Dr. Joshua Vaughan.

His further goals are to be a successful professional engineer and with the attained knowledge to add something to science and society.